TRIBHUVAN UNIVERSITY

INSTITUTE OF ENGINEERING

PULCHOWK CAMPUS

THESIS NO.: M – 336 – MSREE – 2018 – 2022

Optimal Sizing and Performance Analysis of Solar PV-Micro hydropower Hybrid System in the Context of Rural Area of Nepal

by

Deependra Neupane

A THESIS SUBMITTED TO

THE DEPARTMENT OF MECHANICAL AND AEROSPACE ENGINEERING

IN PARTIAL FULFILLMENT OF THE REQUIREMENTS FOR THE

DEGREE OF MASTER OF SCIENCE IN

RENEWABLE ENERGY ENGINEERING

DEPARTMENT OF MECHANICAL AND AEROSPACE ENGINEERING

LALITPUR, NEPAL

MARCH, 2022

COPYRIGHT

TRIBHUVAN UNIVERSITY

INSTITUTE OF ENGINEERING

PULCHOWK CAMPUS

DEPARTMENT OF MECHANICAL AND AEROSPACE ENGINEERING

The undersigned certify that they have read and recommended to the Institute of Engineering for acceptance, a thesis entitled **"Optimal Sizing and Performance Analysis of Solar PV-Micro hydropower Hybrid System in the Context of Rural Area of Nepal"** submitted by Mr. Deependra Neupane in partial fulfillment of the requirements for the degree of Master of Science in Renewable Energy Engineering.

_____

Supervisor, Dr. Nawraj Bhattarai
Associate Professor
Department of Mechanical and Aerospace Engineering

_____

Supervisor, Sanjaya Neupane
Assistant Professor
Department of Mechanical and Aerospace Engineering

_____

External Examiner, Dr. Bishal Silwal
Assistant Professor
Department of Electrical and Electronics Engineering, Kathmandu University

_____

Committee Chairperson, Surya Prasad Adhikari, PhD
Associate Professor and Head
Department of Mechanical and Aerospace Engineering

Date: March 21, 2022

ABSTRACT

Stand-alone hybrid energy systems are an enticing option for electrification in remote areas in several aspects such as grid extension difficulty, economic feasibility, and reliability. The use of existing micro-hydropower (MHP) with other renewable resources in rural areas has not been well studied. Moreover, it is challenging to use mathematical optimization algorithms for these kinds of real-world problems, so the derivative-free algorithm is highly sought. In this study, a methodology has been proposed to perform the optimal sizing, financial, and generation uncertainty analysis of Solar Photovoltaic (SPV) based on an MHP is proposed to handle the intermittent power output of the SPV. The analysis is performed in two cases: using storage and without storage. The optimal sizing is performed using the least present value cost and reliability constraint using different derivative-free algorithms. Additionally, the system need to be technically sound and ensure the frequency stability during load and source imbalance. In this study, the Syncronverter (SV) based on a micro hydropower System (MHPS) is proposed to handle the intermittent power output of Solar Photo-voltaic (SPV). The standalone microgrid is modeled in the MATLAB/Simulink environment. The power control form SV is performed using Power Angle Control (PAC) method. Several case studies are performed, and the simulation results show the dynamics of appropriate sharing of power for both the linear and nonlinear loads by the hybrid system. Both the frequency and Total Harmonic Distortion (THD) of load voltage kept within the standard limits. Moreover, the dynamic response of voltage, power, and frequency of the system due to the induction motor load has also been studied.

ACKNOWLEGEMENT

At the very first, I express my sincerest gratefulness to my thesis supervisor, Prof. Dr. Amrit Man Nakarmi, who has assisted me from the starting to the end of the thesis in each and every steps with his valuable knowledge and efforts. Without his proper guidance, this thesis might not have been completed in time.

I would offer my gratitude to Assoc. Prof. Dr. Nawraj Bhattarai, coordinator of Master of Science in Energy System Planning and Management, Pulchowk Campus for providing me the chance to develop my interpersonal skills through pre-presentations and discussions in the classroom. Additionally, I would like to thank Ass. Prof. Sanjaya Neupane, Deputy Head of Department Mechanical and Aerospace Engineering, Pulchowk Campus for his great support, motivation and supervision throughout my research period.

I would like to thank the Asst. Prof. Dr. Samundra Gururng for providing me guidance for my study and developing the research framework.

I would also like to express my appreciation to Mr. Nabaraj Poudel for his valuable guidance for the analysis in results in my research work. I am also grateful to the teachers of mechanical engineering department, my classmates of 074-MSREE batch, my family members for their valuable guidance and support during my thesis research.

Table of Contents

List of Figures

List of Tables

CHAPTER ONE: INTRODUCTION

1.1.Background

As a principal energy resource, fossil fuels such as coal, oils, and natural gas are heavily exploited globally. The dependence on fossil fuels in the 20th century causes the escalation of climate change. Renewable energy resources (RES) are the alternative option for reducing these carbon footprints, one of the significant causes of climate change. The major three resources RES used widely are hydropower, wind energy, and solar energy. Renewable energy resources have been applied in many countries with significant generation share in their electricity market (Samir M Dawoud et al., 2018; *Renewable Power Generation Costs in 2019*, 2020). Though being environmentally friendly, these energy resources, such as solar, wind, etc., possess a significant drawback on their nature of availability, which is typically uncertain.

Fortunately, the issues given rise by the variable nature of these resources can be partly overcome by integrating the two resources in the proper configuration. This can be achieved by utilizing the qualities of one source to restrain the shortcoming of the other (Sinha et al., 2017). These systems that incorporate multiple renewable energy resources are termed hybrid systems. With the improvement of technologies, they are turning into one of the promising ways to satisfy the electrification requirement in rural area (Kusakana et al., 2009; Razmjoo et al., 2019). However, there are several configurations of a hybrid system that may combine more than two energy sources to supply the load. In the context of a micro-hydro-solar hybrid system, the appropriate size of solar PV and MHP are connected to fulfill the demand.

Moreover, the existing MHP in rural areas can be reinforced with the application of solar PV to cope with rising demand. Generally, this system may encounter frequency imbalance due to load and generation fluctuations without an appropriate storage system. This may result unwanted tripping and outages. However, these hybrid systems that are having generating units combined with battery backup can attenuate their individual fluctuations and improves the system efficiency significantly (Bocklisch, 2015; Vuc et al., 2011). Despite these facts, the sizing of the hybrid system components needed to supply the varying load demand has to be economically practicable. Hence, the optimal sizing of the micro-grid component has to be performed. For this, an appropriate mathematical formulation of the optimization problem needed to be performed and solved that would give the optimal sizes and capacities of the hybrid system’s components.

In summary, the process of developing technology to use renewable energy sources at a small scale that is cheap and can meet the needs of people is still emerging and developing (Syahputra et al., 2021). Among all renewable sources, Solar Photovoltaic (SPV) systems-based hybrid systems and distributed generations are seemingly getting popularity all over world (S. Singh et al., 2016). This is primarily supported due to its simple design and long operation life (Rahimpour et al., 2019). Furthermore, SPV system do not produce any further pollution during energy production. Similarly, Micro Hydro Power (MHP) based distributed generations has been one of the great solutions for the areas having adequate water flow and appropriate geographical gradient. MHP on themselves are simple in construction, easy operatable, clean, cost-effective, and generates almost constant electrical supply. Hence, micro hydro energy technology can be considered for the source electrification for rural areas in less developed countries (Anaza et al., 2017). However, renewable resources possess their own merits and demerits in their application for power generation.

1.2.Statement of Problem

Despite the fact of its popularity, solar power sources possess major drawbacks of power generation uncertainty as the power from the solar resource is environmentally dependent. In an isolated SPV system, the power fluctuation results in frequency deviation (or requires complex circuitry and control system to balance the frequency and load) in the system. This results on poor reliability of the system. The battery system with SPV, which is the most mature and the cheapest energy storage has been found in many applications. This includes, application in load frequency regulation (Akshay et al., 2019), power loss reduction in distribution grids (Lazzeroni et al., 2019), and peak shaving applications (Boyouk et al., 2018). Similarly, as a major drawback of load-frequency imbalance and poor reliability due to overloading has been discouraging the isolated MHP in rural areas. (Maharjan et al., 2014; Murni et al., 2012). This has resulted not only reduction of the life of the system but ultimately shut down the plant. Moreover, in Electronic Load Controller (ELC) based micro hydro system, the generator has to be supplied with rated discharge throughout the time that causes a substantial loss of power in a dummy load.

1.3.Objectives

1.3.1. Main Objectives

The major objective of this study is to provide a financial analysis for integration of solar PV with micro-hydro power to provide reliable, efficient and low-cost electrical supply. Moreover, to analyze the technical absurdities of the hybrid system and providing the appropriate technical specification of the hybrid system.

1.3.2. Specific Objectives

The specific objectives are:

I. To find the optimal size of the hybrid components i.e., size of solar PV and micro hydro-power. Also, to find the optimal size of storage system for storage-based system.
II. To compare the financial and energy generation characteristic of the storage and without storage based proposed hybrid system.
III. To determine the technical characteristic of the proposed hybrid system to find the parameters using appropriate simulation technique. These being specific objective, the study will also take account of financial assessment of proposed hybrid system in the stochastic scenario case of solar irradiance to find the cost of uncertainty.

1.4.Justification of the research

The development of hybrid system requires the sizing of multiple energy resources together that would meet the required load demand of the system. However, the sizing is not an easy task where we have to build a generation model of each component that would be adequate enough to supply the load. Moreover, the sizing has to be both economically as well as technically sound. Hence, the sizing of components in a micro-grid is basically a optimization problem which has to solved to obtain the economically viable combination of generation system in the grid. Moreover, the proposed system has to be technically feasible. Technically feasible means the system should meet the appropriate standard in the aspect of power, voltage frequency and soon. In order to perform the technical feasibility, performance analysis to be done. This can be done be simulating the whole system and observing the performance. Additionally, the system performance can be validated using real time experiment or prototype after simulation. This study has comprised all the method to optimally size the Solar PV and Micro-hydro based hydro system with their technical performance analysis.

1.5.Limitation to the Research

The study may be intervened by different difficulties and limitations. Some of the limitations are listed below.

I. The study will be primarily limited by the availability of secondary data. The resource data for the irradiance is based on meteorological data for a year. Similarly, the discharge data has been taken for a year. This scenario can be different for different years.
II. The study will be limited within the yearly data of the resources. In major, the loading data used for the analysis has been taken for a week of the existing site. The seasonal effect of the load variation, in general it does not deviate too much for isolated system, has not been considered.
III. The study has not considered the temperature effect of the solar PV.
IV. The performance analysis is based on the preset standard models of the system which could slightly differ with the real time implementation of the system.

CHAPTER TWO: LITERATURE REVIEW

2.1.Micro-grid Technologies and Developments

Micro-grids are the Distributed Energy Resource where loads are connected and centrally controlled. The operation of the microgrid is defined for a limits and boundaries where the operation is performed. It may be active power loading, reactive power loading, frequency and voltage drops (Fusheng et al., 2016). Generally, microgrid can be standalone or grid connected. In recent years, micro-grids have been developed as one of the most promising way for rural electrification. Generally, the cost of transmission to the areas are overcome by developing the microgrids in the areas. Moreover, the availability of grid on the location having microgrid can be interconnected to the grid.

The conceptualization and development of microgrid had been started back from 2001. However, within just ten years, microgrid technologies have been developed to integrated variable generation sources such as solar photovoltaic with storage systems. (Ton et al., 2012), (Marnay et al., 2015) are the early stematic research and development programs that began in the Consortium for Electric Reliability Technology Solutions (CERTS) effort in the United States (R. Lasseter et al., 2002). Similarly, in the MICROGRIDS project in Europe (Hatziargyriou et al., 2006). In 1999, CERTS began to recognize the origin of grid connected microgrid concept (R. H. Lasseter et al., 2004)(Hatziargyriou et al., 2006). Nowadays, several countries have prepared and proposed standards for developing and constructing the micro-grids.

With the development of advanced computer system, information technologies and communication technologies, the microgrids are turning in to more flexible, cleaner and more economics smart grids. However, the developments are still a great topic of research to improve the performance stability and operation. With the use of distributed generators and micro grids, the losses of the feeder also found to be decreased. Moreover, the microgrid improves the system efficiency with optimal energy management techniques.

2.2.Optimal Sizing of Micro-grid Components

Many researchers have performed studies that concern hybrid micro-grid. From the investigation, it has been confirmed that the hybrid renewable energy system gives a good performance and a lower cost compared to the single individual resources in the system (Beshr,

2013; Celik, 2002; Kusakana et al., 2011). Several studies have been done on finding the optimal sizes in a hybrid system. The optimization has been performed using different software platforms and using several algorithms (Samir M Dawoud et al., 2018). Kenfack and colleagues have studied the sizing of a small hydro-PV-hybrid system for rural electrification in developing countries using Homer software (Kenfack et al., 2009). Himadry and colleagues have proposed PV/tidal powered micro-hydro and diesel hybrid system: A study on southern Bangladesh using HOMER Simulation (Das et al., 2016). Kusakana and colleagues have studied the feasibility of a hybrid PV-Micro Hydro system for rural electrification in Kwa-Zulu Natal (Kusakana et al., 2009). Similar pieces of literature on the feasibility study and optimal sizing that are performed using the HOMER software platform are the study done by Dawoud et al., Sone et al., and Kumar et al. (Samir Mohammed Dawoud et al., 2015; Y. V. P. Kumar et al., 2014; Soni et al., 2014). Apart from commercial software, using heuristic optimization algorithms such as particle swarm optimization (PSO) and genetic algorithm (GA), several studies have been done to determine the optimal sizes in hybrid systems. Yang and colleagues had studied the optimal design and techno-economic analysis of the hybrid solar-wind system using GA (Yang et al., 2008, 2009).

Similarly, a methodology has been proposed for optimal sizing of the hybrid wind-solar system by Koutroulis et al. and Xu et al. using GA (Koutroulis et al., 2006; Xu et al., 2005). Moreover, Mohammadi and friends used GA for optimal sizing of microgrid under the pool and hybrid electricity markets (Mohammadi et al., 2012). The Particle Swarm Optimization (PSO) algorithm for optimal sizing and economic analysis has been a popular method for so long. Moghaddas et al. has studied optimal sizing of a stand-alone hybrid system using PSO (MoghaddasTafreshi et al., 2007). Similarly, using this algorithm, optimal sizing of PV- Wind hybrid system consisting of diesel generators has been performed by Boonbumroon and colleagues (Boonbumroong et al., 2011). In addition, Jayachandran et al. used PSO for sizing optimization of the hybrid micro-grid system (Jayachandran et al., 2017). Kumar and colleagues have studied the sizing optimization of PV/MHP-based hybrid energy systems in the rural area of Western Himalayan Himachal Pradesh in India using PSO (S. Kumar et al., 2019).

The optimization problem of optimal sizing using a storage-based micro-grid system is non-convex and nonlinear (Zolfaghari et al., 2019). The process of convexification to find one optimal solution, which is globally optimal, is complicated. Hence, using appropriate

derivative-free stochastic algorithms can be used to solve the problem easily. But, stochastic optimization algorithms such as PSO, GA do not give the real global solution. Hence, the solution differs for every execution of the optimization algorithm.

Moreover, a particular optimization algorithm for a problem does not mean it would fit in any case. Hence, a comparison of multiple optimization algorithms can be checked and compared to find the best-suited one. This study has compared multiple algorithms applied for the proposed hybrid system to find the optimal sizes of SPV and MHP.

Moreover, for the optimal sizing of components on a micro-grid, the uncertainty on resources such as solar GHI, wind speed, etc., has to be considered for risk minimization. Unfortunately, in the case of the SPV-based MHP hybrid system, the study is missing. Hence, we have conducted this study to fulfill the gap mentioned above.

This study has been undertaken with formulating a power generation model of Solar PV, MHP, converter, load controllers, and storage system. For optimal sizing, per unit and/or kW costing, including investment, replacement, and operation and maintenance, each component has been used to formulate the objective function. As a cost minimization problem, the optimal problem is formulated as finding the sizes for the minimum net present cost of the hybrid system. Similarly, appropriate constraints have been developed that define the generation and load balance criteria, i.e., outages and lower and upper limits of optimization variables. The optimization problem has been treated with three derivative-free optimization algorithm. The best result, i.e., minimum solution, is taken for further analysis. The financial analysis for the optimal sizes has been performed. And finally, the effect of variability of solar generation has been studied using a statistical model.

2.3.Performance Analysis of Micro-grid

Standalone hybrid system is getting popular to provide the electricity requirements in rural areas. As the cost of grid extension in rural areas is high due rough terrain and disperse settlements, these system has a typical advantage on the rural area (Kusakana et al., 2009; Razmjoo et al., 2019). Hybrid energy systems with renewable energy resources are more encouraged as they have a much lower environmental impact than the systems with conventional energy resources. Moreover, renewable energy source (RES) based hybrid system additionally reduces the possibility of source-load imbalance due to the environmental dependency of renewable resources on power generation. Among several RES based hybrid systems, solar and MHP hybrid system can solve the deformities of both systems, SPV and

MHP as discussed earlier, in terms of frequency imbalance and power losses. The power loss in the ballast load of MHP can be reduced by releasing the discharge at the scheduled time to some other purpose, for instance irrigation in rural areas. While the frequency imbalance can be solved by sharing appropriate loads by both systems during source uncertainty or load uncertainty.

Hence, Thus an SPV system consisting of an SPV array with converters, harmonic filters, and a MHP plant consisting of hydraulic turbines, a synchronous generator, and electronic load controller is integrated into solar microhydro hybrid power system (SMHPS). The efficiency and reliability of the SMHPS mainly depend upon the control strategy of the converter on SPV side and the load controller in the MH side. The nature and performance of SPV is quite different in terms of physical and electrical characteristics than that of synchronous generators used in MHP. Hence, the SPV penetration effects on the frequency stability of the system (Liu et al., 2017). Moreover, the use of power electronics-based devices like voltage source converter and electronic load controller creates voltage and current distortion in system.

Due to several advantages of SV as a converter such as availability of voltage and frequency droop mechanism, it provides greater flexibility on its application on microgrids (Cheema, 2020). Furthermore, the inherent inertial characteristic of the SV can provide services as frequency support and transient power sharing as primary control actions (D'Arco et al., 2015). SV based power converter operates as a voltage source connected to the grid and can supply fault currents, as well as unbalanced and harmonic currents to non-linear loads (Bignucolo et al., 2018). Moreover, SV based system can reduce the rate of change of frequency in the system that has high penetration of variable renewable energy generation sources (Bignucolo et al., 2018) and possess automatic synchronisation ability (Yap et al., 2019).

Several studies have been performed on using the SV as a converter for the renewable source integration in grid/microgrid. Monila et.al. have presented the method for reference power variation in the syncronverter based using the voltage fluctuation using a PI controller (Amin et al., 2016). Chandrakar et.al. have studied the grid integration of solar PV using SV. Apart these, Mesharam and collegures have studied the solar and microhydro using induction machine as microhydro power source (Meshram et al., 2014). Similary, Chaudary et.al have presented the power angle control strategy for synchronization and power flow control in microgrid (Chaudhari et al., 2015). Moreover, Yong and colleuges have applied the power

angle variation method to obtain power flow control in a distribution generation(Xue et al., 2009). The Svensson and friends have used the power angle control strategy in wind energy for grid integration(Svensson, 1995).

This study has introduced the power-sharing of SV based SPV with a MHP hybrid system using the power angle variation method. The synchronous generator in grid-connected or isolated MHP system provides greater advantages and flexibility compared to the induction machine (Freitas et al., 2006). Hence, this study presents a theoretical basis of a hybrid system using synchronous machine in MHP and SPV in SV as a power source. The modeling and simulation are carried out under MATLAB/SIMULINK environment. The effect of load variations, source variation (irradiance level in SPV) on voltage profile, harmonics and sharing proportion has been studied. Similarly, the effect of the use of induction motors on the proposed hybrid system is analyzed.

CHAPTER THREE: METHODOLOGY

3.1.Solar PV-MHP Hybrid System Sizing and Optimization

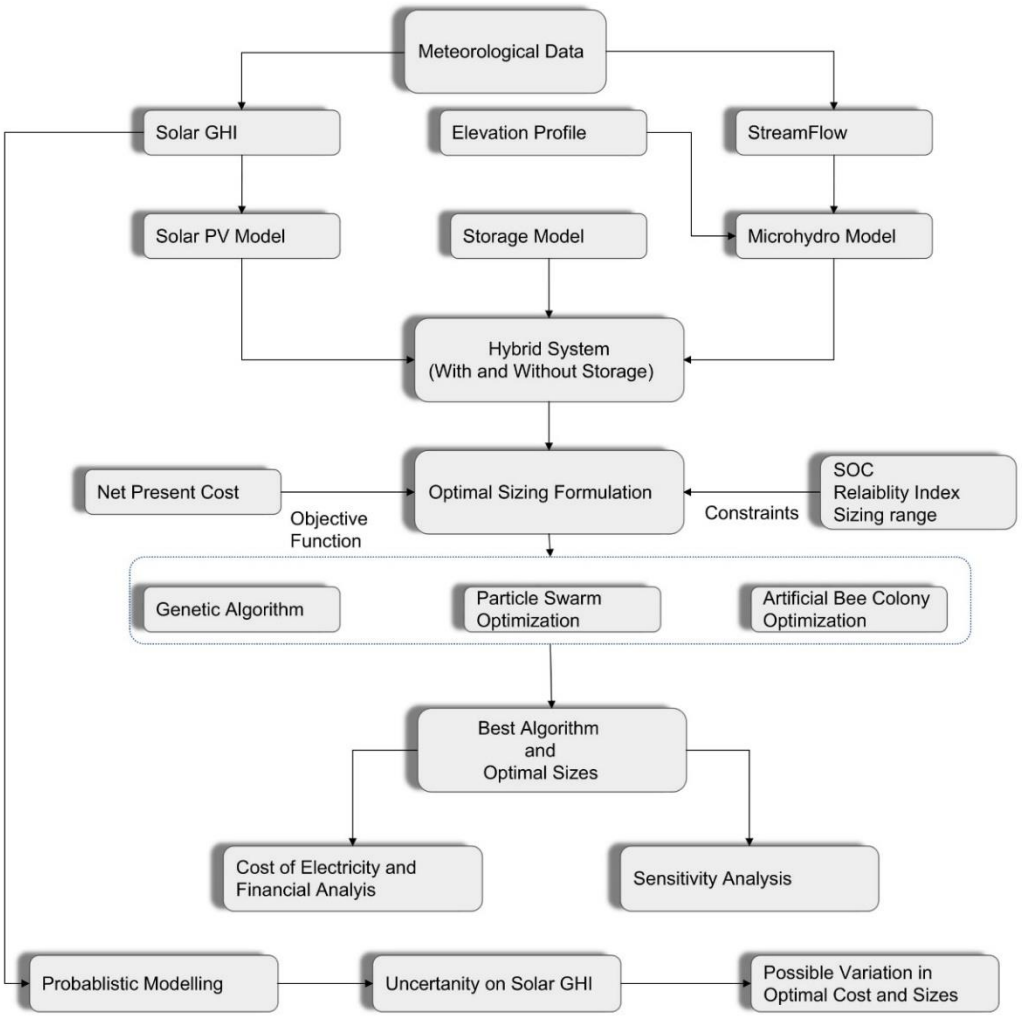

Figure 1: Methodological Framework of the study for optimal sizing of the proposed hybrid system.

3.1.1. Power Generation Modelling for Optimal Sizing

3.1.1.1.Solar PV Modelling

The PV system's design entails calculating the number of standard-size PV modules required to convert sunlight to electricity. Then, the power generation from the SPV module (PPV) is calculated using Eq. (1).

$$P_{PV} = 1000 \times \mathrm{G} \times P_{PV,rated} \times \eta_{PV,conv} \quad (1)$$

where G is the global horizontal irradiance on the surface of each array (W/m2), and Ppv,rated is the rated power of each array which is taken as 1 kWp such that G=1 kW/m2. Also, ηpv,conv

is the efficiency of the DC/DC converter between each array taken as 0.95(N. M. Pearsall, 2017). The investment capital cost is taken as 618 USD/kWp with a fixed operation and maintenance cost of 10 USD/kWp (*Renewable Power Generation Costs in 2019*, 2020), and lifetime of the project is taken as 25 years.

3.1.1.2.MHP Modelling

The power generation from the micro-hydro depends on the total head, streamflow discharge available, and the system's overall efficiency. Once designed for a particular discharge, the power output of micro-hydro mainly depends on the available discharge and turbine efficiency at the part flow. The general model for MHP generation (Pmhp) is calculated using Eq. (2).

$$P_{mhp} = \eta_{mhp} \times \gamma \times q_{des} \times H_{des} \; if \; q \geq q_{des} \quad (2)$$

$$= \eta_{mhp} \times \gamma \times q \times H_{des} \quad if \; q < q_{des}$$

where ηmhp is the overall efficiency of the MHP taken as 0.5 (Harvey et al., 1993; KRISTOFERSON et al., 1986) that includes the efficiency of the turbine, generator, and head loss, γ is the specific weight taken as approximately 1,000 kg/m3, q is the discharge available which is less or equal to design discharge qdes and Hdes is the design gross head. The installation cost for the construction of a MHP plant is taken as 1,779 USD/kW and maintenance cost of 5 percent of investment cost, using the data collected by Vaidya and colleagues (Vaidya, 2014). The study has included the cost per kW of MHP at seven different places in Nepal, which gives the average cost per kW of MHP as approximately 1,888 USD/kW considering the civil, generator equipment, and line. However, the study has also studied the projects under the Renewable Energy Development Programme (REDP) support that comes from 1,279 to 1,779 USD/kW. Hence, with considering the cost per kW of MHP with support, we have taken the upper range value per kW cost of MHP with subsidy in this study.

3.1.1.3.Battery Storage Modelling

Batteries are the generally used energy storage system in microgrid systems. Lead-acid batteries are cost-effective and have good electrical characteristics(Garche et al., 2013) and are generally used in the microgrid system. To investigate the charge and discharge characteristics requirements in the hybrid system the battery's state of charge can be modeled. The state of charge gives the availability of the power at any instant.

SOC(t), the preceding state of charge, and the energy degradation or buildup from state t-1 to state t are all tied to the battery's state of charge (SOC(t)) at any hour t of the year. During

surplus energy in the system, the battery stores energy and supplies during the deficient condition. The state of charge of the battery at any instant of time can be written mathematically for two scenarios, viz. charging and discharging, given by Eq. (3) and (4).

- If $P_g(t) = P_{PV} + P_{mhp} \geq \frac{P_l(t)}{\eta}$, the generated renewable power at any time step (Pg(t)) is sufficient to satisfy the load demand Pl(t) (with added losses), and the excess is stored in the battery bank. The excess energy above the rated capacity of the battery will be dissipated to ELC. In this case, the battery is claimed to be in the process of charging, and SOC(t) is given as Eq. (3) (Ramoji et al., 2014).

$$SOC(t) = SOC(t-1) \times (1-\sigma) + \frac{(P_g(t) - \frac{P_l(t)}{\eta_{inv}}) \times \eta_{bc}}{1000 \times N_b \times C_b} \quad (3)$$

Where, ηbc is the charging efficiency of the battery taken as 0.9 (Adaramola et al., 2014), ηinv is the inverter/converter efficiency, which is taken as 0.9 and respectively. Similarly, σ is the hourly self-discharge rate of 0.01 % per hour, an average value for lead-acid batteries (Garche et al., 2013).

- If $P_g(t) = P_{PV} + P_{mhp} \leq \frac{P_l(t)}{\eta}$, the generated renewable power would not be is sufficient to satisfy the load demand, and the excess power requirement is provided from the battery bank. In this case, the battery is said to be in discharging stage, and SOC(t) is given as Eq. (4) (Ramoji et al., 2014).

$$SOC(t) = SOC(t-1) \times (1-\sigma) + \frac{(\frac{P_l(t)}{\eta_{inv}} - P_g(t)) \times \eta_{bd}}{1000 \times N_b \times C_b} \quad (4)$$

Where ηbd is the discharging efficiency of the battery taken as 0.9 (Meyer, 2004). Similarly, Nb is the amount of batteries n number, and Cb is the capacity of each battery having a nominal capacity of 2.42 kWh with a maximum depth of discharge (DOD) of 80 % (Atieh et al., 2018).

Over-discharge and under-discharge should be avoided if we want your batteries to last longer. Consequently, at any hour t, SOC(t) should be subjected to the constraint using depth of discharge (DOD) represented by Eq. (5).

$$(1 - \text{DOD}) \leq \text{SOC(t)} \leq 1 \quad (5)$$

The battery storage system is modeled as a generator. Similarly, the power output depends on the current state of charge and the previous state of charge of the battery. The power supplied by the battery for any instant of time t is given by Eq. (6).

$$P_{bat}(t) = (SOC(t-1) - SOC(t)) \times \eta_{bd/bc} \times N_b \times C_b \quad (6)$$

The power (supplied to the system) will be positive while discharging and negative while charging. The investment and replacement cost of a battery unit of capacity specified above is taken as 200 USD per unit. The lifespan is taken as 5 years (Adaramola et al., 2014).

3.1.1.4.Electronic Load Controller Modelling

The variation in load needs to be balanced by using an appropriate power control mechanism. In MHP, an induction generation controller or electronic load controller is used. The electronic load controllers (ELCs) are generally used in micro-hydro installations, which divert excess power to a dump load to regulate voltage and frequency. The excess power dumped at any instant in ELC is modeled as per Eq. (7).

$$P_{elc}(t) = P_{mhp}(t) + P_{pv}(t) + P_{bat}(t) - P_{load}(t) \quad (7)$$

Where Pmhp is the power generated by MHP given by Eq. (2), Ppv is the power generated by SPV given by Eq. (1), Pbat is the power generated or consumed by battery given by Eq. (6), and Pload is the total load at any instant hour. The power generated or consumed with the battery depends on SOC's previous and current value, as discussed in sub-section 2.1.3. Hence it can be positive when discharging and can be negative while charging. For a fully charged or fully discharged case, Pbat will be zero. ELC balances the total supply and demand by varying the power in a dummy load. The positive value of Pelc means that the excess power (after charging the battery) is discharging in ballast load. However, a negative value on ELC power means the system has an outage due to power deficiency. The installation cost of ELC is taken as 150 USD/kW, and annual operation and maintenance is taken as 5 percent of the total installation cost with a total lifetime of 25 years. This data is taken from the survey of market rates of ELC in markets in the year 2020.

3.1.1.5.Inverter/Converter Modelling

In Eq. (3) and (4), ηinv is the inverter or converter efficiency. The converter converts the excess ac energy to dc to charge the battery. Similarly, during energy deficiency, the inverter converts the dc to ac to supply the load. In this study, the inverter is used as a general term for both one (i.e., inverter and converter). The investment cost of the inverter is taken as 200 (USD/kVA)(Fu et al., 2018), Replacement cost: 200 (USD/kVA), with no annual cost of repair and maintenance, lifetime as 10 years, and efficiency as 90% (Yimen et al., 2020). The power factor of the inverter is taken as 0.85 to convert actual kVA and to kW power.

3.1.2. Optimization Problem Formulation

The optimal hybrid system sizing is determined by minimizing the total net present cost of the hybrid system. The optimization is performed by taking the hourly average irradiance data, discharge data, and loading data for a year for a location. The hybrid system consists of PV arrays, micro-hydro, load, converters, and electronic load controller. The system should meet the demand for every timestamp. The costs can be minimized, and the components have the optimal sizes. Optimization variables are the PV size, design head of the micro-hydro (after head losses), and design discharge of micro-hydro (after seepage losses). For the calculation of system cost, Net Present Cost (NPC) is chosen. In this study, only the capital investment cost, operation, maintenance, and replacement cost have been used for determining NPC. The NPC for the system is shown in Eq. (8). We have not considered the hybrid system's revenues after operation to determine the NPC during optimization. This would reduce the complexity of the objective function.

$$NPC_i = N_i \times (CC_i + K_{ib} + K_{ii} + OMC_i \times \left(\frac{1}{CRF(i_{r,}n)}\right)) \quad (8)$$

Where N is the capacity (kW) or the number of units (for storage) of each ith component, CC is the capital cost (USD/Unit), and OMC is the operation and maintenance cost of the components. Additionally, Kib and Kii is the replacement cost of battery and inverter respectively as the single payment present worth, R is the life span of the project, it is the real interest rate. Also, CRF is the capital recovery factor which is defined by Eq. (9).

$$CRF(i_r, n) = \frac{i_r(1+i)^n}{(1+i)^n-1} \quad (9)$$

Only the batteries and converters are replaced during the system's lifetime. Batteries are replaced four times (5th, 10th, 15th, and 20th), whereas converters are replaced twice (10th and 20th). Hence, the Ki for batteries and converters is given by Eq. (10) and (11), respectively.

$$K_{ib} = RC_b(\frac{1}{(1+i)^5} + \frac{1}{(1+i)^{10}} + \frac{1}{(1+i)^{15}} + \frac{1}{(1+i)^{20}}) \quad (10)$$

$$K_{ii} = RC_{inv}(\frac{1}{(1+i)^{10}} + \frac{1}{(1+i)^{20}}) \quad (11)$$

Where RCb and RCinv are the replacement cost of battery and inverter.

The loading and generation have to be balanced for each timestamp in the system. Otherwise, a power outage will occur in the system. This type of outage has to be minimized for the reliable

operation of the hybrid system. In this study, the reliability index of the Equivalent Loss Factor (ELF) has been taken for determining the reliability of the proposed hybrid system. The ELF is shown in Eq. (12).

$$ELF = \frac{1}{H}\sum_{t=1}^{H}\frac{Q(t)}{D(t)} \qquad (12)$$

Where H is the total time steps under consideration, Q(t) is loss of load, and D(t) is demand at the step time (Ardakani et al., 2010). The constraint of ELf ≤ 0.02 is used, which is the typical value for a stand-alone hybrid system in rural areas (Ardakani et al., 2010). The loss of load for t step of time is calculated based on Eq. (13).

$$Q(t) = \left[\frac{G(t)}{1000} \times P_{pv,opt} \times \eta_{pv,con}\right] + \left[\eta_{mhp} \times \gamma \times q(t) \times H_{opt}\right] + \left[\left(SOC(t-1) - SOC(t)\right) \times N_b \times C_b \times \eta_{inv}\right] - P_{load}(t) \qquad (13)$$

As already mentioned, the objective function is the net present value of the total system given by Eq. (14), and the constraints for the optimization problem are summarized with the objective function.

$$J = min_x \sum_i NPC_i \qquad (14)$$

Subjected to:

- $0 \leq q_{des} \leq 2$
- $0 \leq H \leq 40$
- $0 \leq P_{pv} \leq 50$

For storage-based system

- ELF = 0
- (1-DOD) ≤ SOC ≤ 1
- $0 \leq N_b \leq 60$

For a non-storage-based hybrid system

- ELF ≤ 0.02

The decision variables are used to determine the installed capacity of solar, MHP, battery, and inverter sizes that have been modeled in the above sections.

3.1.3. Financial Analysis

Financial analysis is performed by determining the yearly cash flow for both systems. The cash flow includes the annual revenue generation and expenses (operation and maintenance costs). As the application of the hybrid system primarily focuses on the context of a residential area of rural areas, the major electricity supply would be a single phase. This would generate revenue after the operation of the hybrid system. The tariff rate of USD 0.073 per kWh (converted using conversion price for the year 2020), the weighted average unit energy cost for the single-phase is taken using the tariff rate of country Nepal (NEA, 2018). Yearly revenue generation in the system has been determined using the energy cost. Several indicators such as simple payback, discounted payback, benefit-cost ratio (BCR), and internal rate of return (IRR) have been calculated for both of the systems and compared.

Moreover, the Levelized cost of electricity (LCOE) has also been determined. The LCOE is calculated for the system using Eq. (15). In addition, the curtailment of energy for a year, i.e., the total energy wasted and dissipated in ELC, has also been studied, which can be used for grid supply after its availability that would further increase the revenue of the system.

$$LCOE = \frac{\sum_i [(CC_i + K_i) \times CRF(i_r, n) + OMC_i]}{E_{Agen}} \quad (15)$$

Where Ki is the total net present replacement cost of replaceable equipment, i.e., battery and inverter for the project life, and EAgen is the annual usable energy generation of the hybrid system. The discount rate is taken as 10 % using the reference of microeconomics Indicators of Nepal (Bank, 2019).

3.1.4. Solution Method

The optimization is performed using derivative-free stochastic optimization algorithms. Popular optimization algorithms such as particle swarm optimization algorithm and genetic algorithm have been used in the study. The results of these optimization techniques were compared to those achieved by employing the Artificial Bee Colony Algorithm (ABC). The Artificial Bee Colony Technique is a heuristic optimization algorithm based on swarms.

3.1.4.1.Genetic Algorithm (GA)

Additionally, genetic algorithm is utilized as a benchmark of past investigations on optimal sizing of the hybrid system done by Yang et al., Koutroulis et al., Mohammadi et al., and Xu et al. (Koutroulis et al., 2006; Mohammadi et al., 2012; Xu et al., 2005; Yang et al., 2008, 2009).

The pseudocode for the genetic algorithm is given below:

Data and Initialization: *population of individuals and fitness function; number of iterations, population and condition of stop*

Result: *Best individuals on applying on the fitness function*

Begin:

t = 0;

Create an initial population – $P_{op}(0)$

Evaluate individuals – Calculate the value of the fitness function for each individual in the population P_0*;*

DO:

Select individuals for the new population $P_{op}(t) - selection$*;*

Perform crossover operation

Perform the mutation of individuals

Evaluate individuals;

t = t + 1;

while: *stop condition reached*

end

3.1.4.2.Particle Swarm Algorithm (PSO)

The particle swarm optimization algorithm is used based on its application in previous studies, such as the study on optimal sizing for the stand-alone hybrid system by Moghaddas and colleagues, Boonbumroong and colleagues, and Kumar and colleagues(Boonbumroong et al., 2011; S. Kumar et al., 2019; MoghaddasTafreshi et al., 2007).

The pseudocode for the particle swarm optimization algorithm is given below:

Data and Initialization: *population, maximum iteration, lower and upper limit for position and velocity and condition for stop.*

Random initialization of the position of particles i.e. $x_{min} \leq x_i \leq x_{max}$

Random initialization of the velocity of particles i.e., $v_{min} \leq v_i \leq v_{max}$

Result: *Best solution on applying the fitness function on initialized population*

Begin*:*

t = 0;

For i: population:

Calculate v_i using following equation

$$v_i = w \times v_i + c_1 \times random(0,1)(p_{best,i} - x_i) + c_2 \times random(0,1) \times (g_{best,i} - x_i)$$

Calculate position x_i using following equation

$$x_i = x_i + v_i$$

If $f_i < f_{pbest,i}$:

$$p_{best,i} = f_i$$

End if

if $f_i < g_{best,i}$ then:

$$g_{best,i} = f_i$$

End if

End for

t = t+ 1

End while

3.1.4.3.Artificial Bee Colony Algorithm (ABC)

The ABC optimization algorithm has been widely used in scientific and engineering problems due to its simple implementation and full exploration and utilization of the natural process of solving complex problems. (Shah et al., 2016).

The pseudocode for the artificial bee colony algorithm is given below:

Data and Initialization: *population and fitness function, iteration, population size, onlooker bees' number and employed bees' number.*

Result: *Best solution on applying on the fitness function*

Begin:

t = 0;

for i = 1: Employed Bees

select a random solution and apply random neighborhood structure;

sort the solutions in ascending order based on the penalty cost;

Determine the probability for each solution, based on following Formula

$$p_i = \frac{\Sigma\left(\frac{1}{fitness_i}\right)^{-1}}{fitness_i}$$

end for

For i:1: Onlooker Bee

sol^* = the solution who has the higher probability;

sol^{**} = apply a random Neighborhood structure on sol^*;

If (sol^{**}< sol_best):

sol_best = sol^{**};

end if

end for

t = t+1;

end begin;

The convergence and accuracy of these algorithms differ in implementation in the characteristics and nature of the problem. In the study, the best results, based on the minimum result on multiple executions done for at least 20 executions, have been taken for optimal sizing. Each of the algorithms is performed with 100 population sizes for 200 iterations. The optimization algorithm that gives the best performance (least minimum value) is applied for further analysis on sensitivity and uncertainties analysis. The algorithms are implemented using the open-source python library mealpy (Thieu, 2020). The study's modeling, analysis, and presentation have been done using the python programming language (van Rossum, 1995).

3.1.5. Sensitivity and Uncertainty Analysis

As shown in Eq. (14), the LCOE of the hybrid system depends on several parameters. Hence, we conduct a sensitivity analysis to understand the dependency of LCOE on these parameters. Particularly, our sensitivity analysis considers a deviation of ± 30% for the base values of investment and operation and maintenance cost of components and interest rate. Moreover, consideration of outages in the system also affects the cost of a hybrid system as it affects the sizing of components. Hence, the effect of ELF on the LCOE of the system has also been studied.

The nature of SPV generation is uncertain, as it depends on solar radiation. However, the streamflow is relatively predictable, and the yearly pattern does not change so much for several years. The uncertainty in the generation of SPV affects the overall sizing of the hybrid system and affects the minimum cost that is determined for a specific year. Hence, SPV generation

uncertainty analysis has been performed to observe the distribution of optimal sizes and the cost of the system. That would be helpful to determine the cost of the uncertainty of the system. For this, the available solar radiation data is fitted with the best probabilistic distribution system. In this study, we have taken three distributions for fitting the hourly irradiance data of the location. And then, Monte Carlo simulation is performed using the probabilistic model. The random GHI for each hour of daytime is generated from the best-fitted distribution for a whole year. And optimization is performed using the best algorithm obtained in subsection 2.4. The uncertainty analysis is performed for both the Storage and non-storage-based proposed hybrid system.

The uncertainty analysis performed in this study is a statistical uncertainty. As we have data set of limited periods of time, we apply some distribution function on the dataset and determine the numerical value for its parameters. In this study we have selected 3 type of distribution function to fit the solar irradiance data. These distributions have been used by several authors that includes the study done by Arthur et.al., Lv et.al. Khatod et.al. Ayodele et. al. , Guwaeder et.al. and son on (Arthur et al., 2013; Ayodele et al., 2015; Guwaeder et al., 2017; Khatod et al., 2009; Lv et al., 2016). to fit the solar irradiance data for statistical analysis.

3.1.5.1.Lognormal Distribution

It is a type of continuous probability distribution in which the random variable's logarithm is normally distributed. For instance, if a random variable x has a lognormal distribution than, z=log(x) has a normal distribution. The probability density function for the lognormal distribution can be written as:

$$f(x,s) = \frac{1}{sx\sqrt{2\pi}} \exp\left(\frac{log^2(x)}{2s^2}\right)$$

3.1.5.2.Beta Distribution

It is also a type of continuous probability distribution. The probability density function for the beta distribution is written as:

$$f(x,a,b) = \Gamma(a+b)x^{a-1}\frac{(1-x)^{b-1}}{\Gamma(a)\Gamma(b)}$$

For $0 \leq x \leq 1, a > 0, b > 0$ *and* Γ *is gamma function.*

3.1.5.3.Gamma Distribution

The probability density function for gamma distribution is given below:

$$f(x, a) = \frac{x^{a-1}e^{-x}}{\Gamma(a)}$$

For $x \geq 0, a > 0\ and\ \Gamma(a)$ refers to gamma function.

These probability densities have been realized using the python SciPy library in this study.

3.1.6. Methods of Data Collection and Analysis

The hourly discharge (streamflow) data is taken for the typical stream of a remote location of the country Nepal. The data is obtained by using HIWAT Stream-flow Prediction Tool for Nepal developed by ICIMOD (*Streamflow Prediction Tool, Nepal*, n.d.) shown in figure 2. For the micro hydropower's head determination, the site's digital elevation model (where the discharge data has been taken) has been used. The data is obtained using the digital elevation data provided by google earth of the location shown in figure 2. Similarly, minute average data for irradiance (GHI), which is later re-sampled for hourly data for a year for the site, is obtained from the meteorological data center, Lumle, that lies nearby the site location shown in figure 3. The load data has been taken from the existing stand-alone micro-hydro site. The load data is taken for a week in an hourly interval shown in figure 4. This weekly data is replicated for the year in the study.

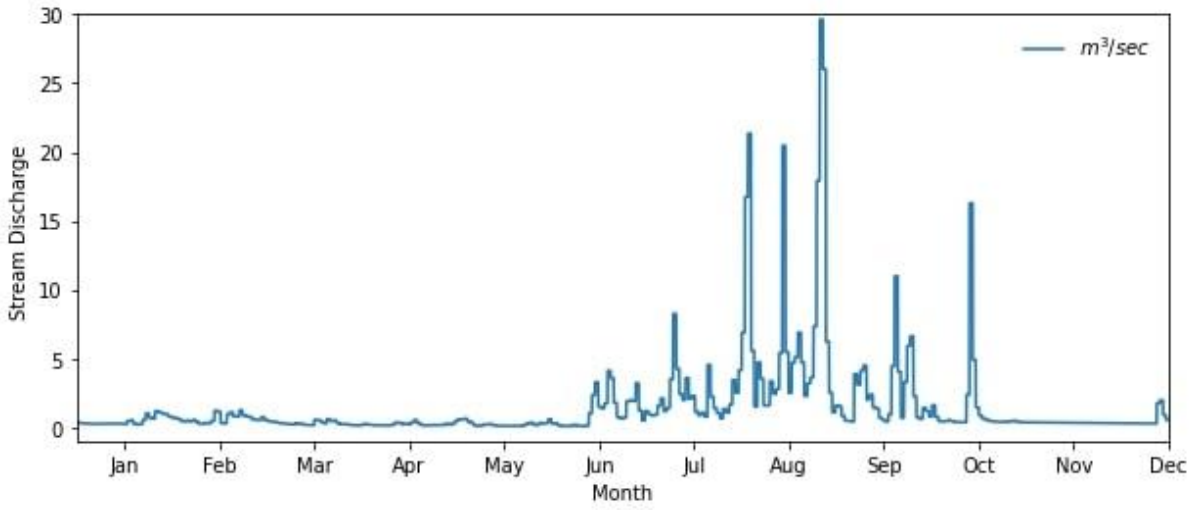

Figure 2: Stream Flow-Discharge characteristic of the stream taken in the study.

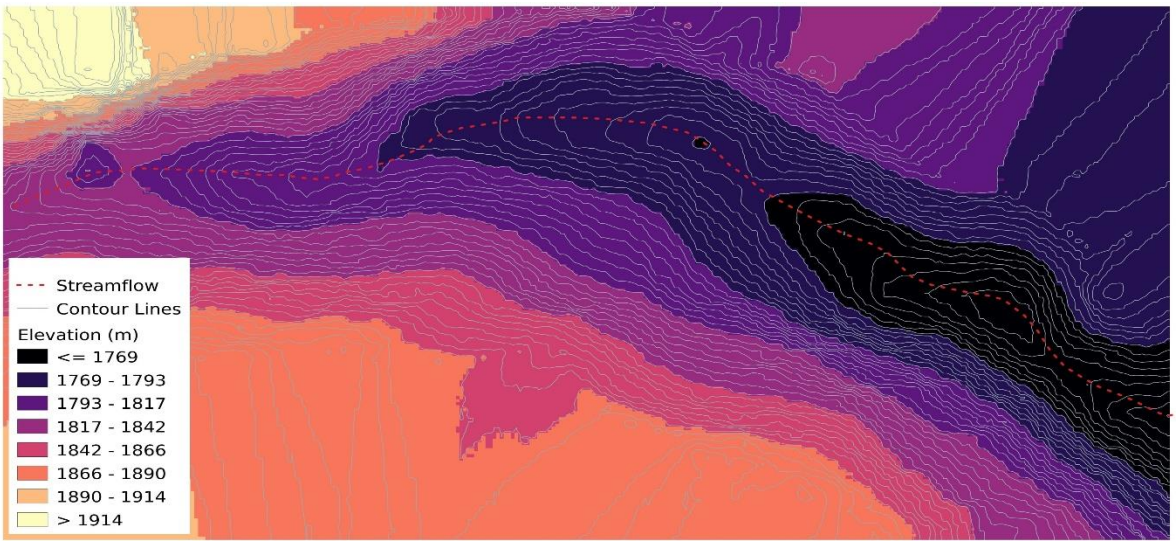

Figure 3: Digital Elevation Model of the site taken in the study.

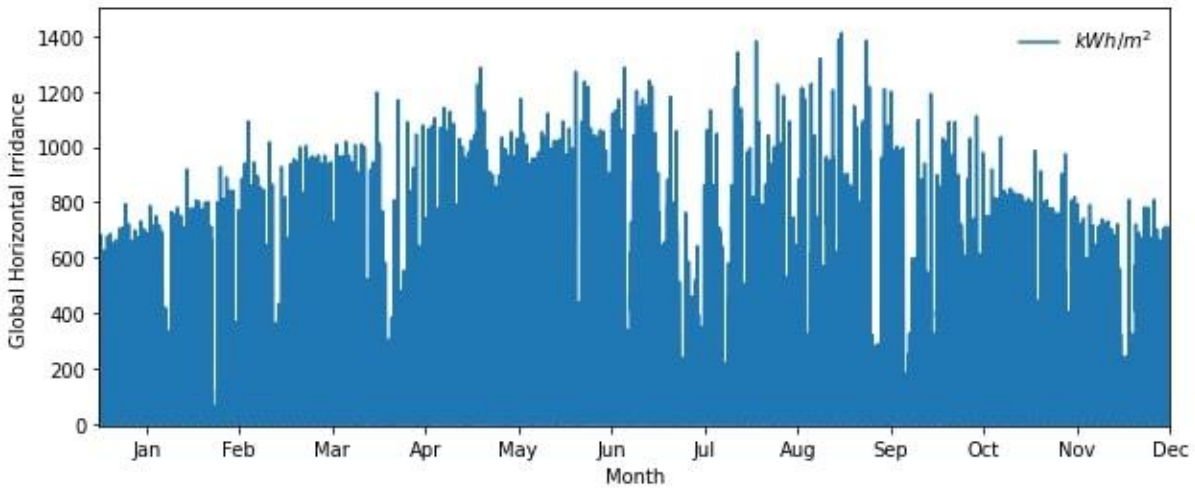

Figure 4: Hourly average solar irradiance (GHI) of the site.

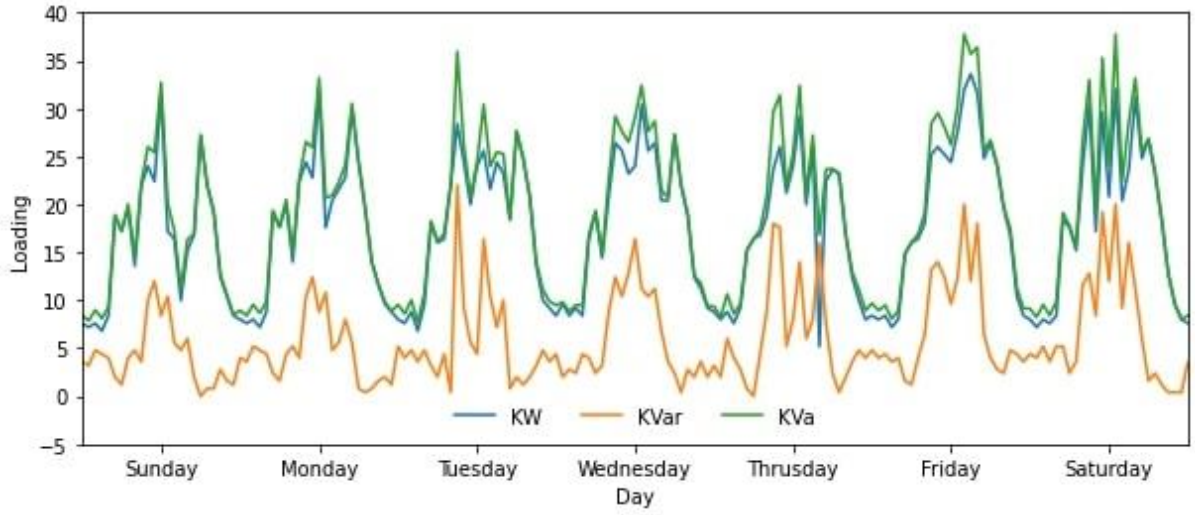

Figure 5: Weekly load profile of a existing MHP based isolated rural area.

3.2. Performance Analysis of Solar PV- MHP Hybrid System

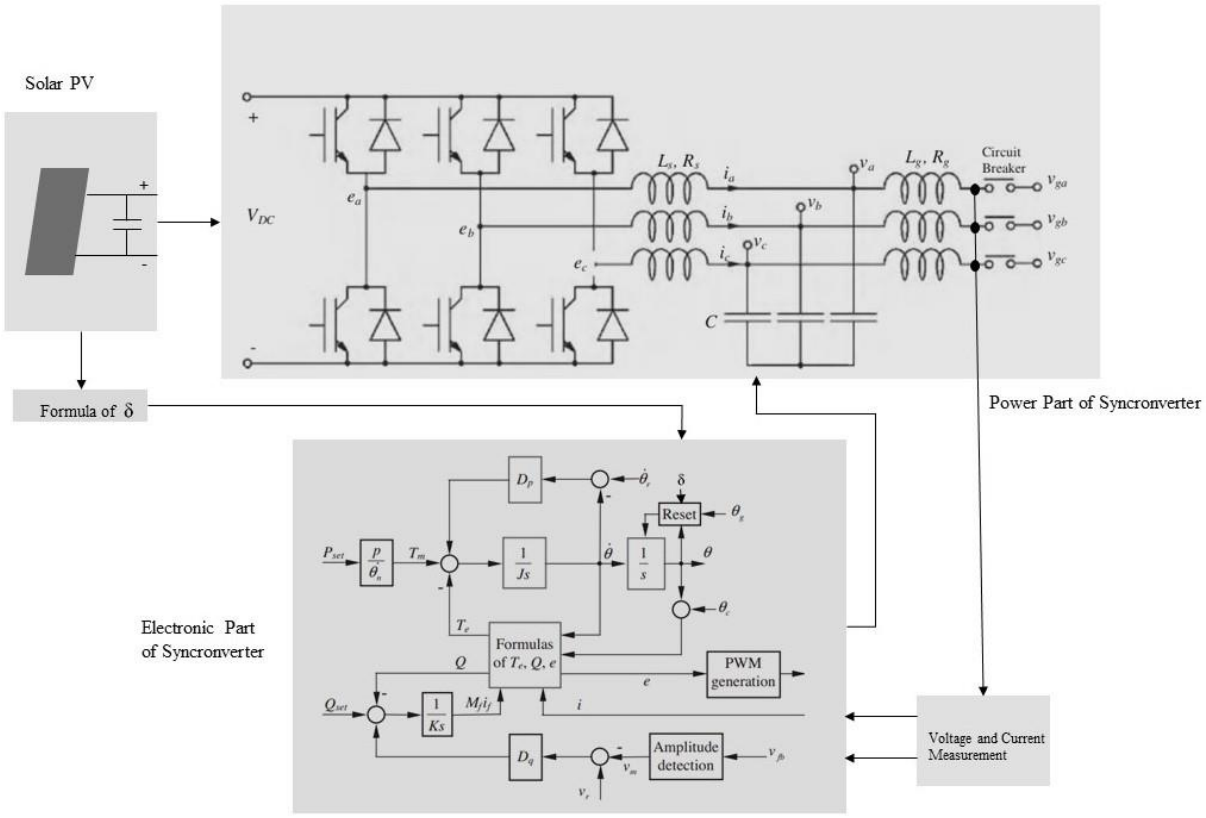

Figure 6: Detail modelling and connection diagram of proposed Solar-MHP hybrid system.

3.2.1. Mathematical Modelling of Components

3.2.1.1.Modelling of Synchronverter

SV is an inverter that can be operated to mimic the behavior of a synchronous generator. The dynamic equations are the same; only the mechanical power exchanged with the prime mover (or with the mechanical load, as the case may be) is replaced with the power exchanged with the dc bus (Zhong et al., 2010). In this study, the SV model suggested by (Zhong et al., 2012) has been used. The SV model is shown in Figure 6 that shows electronic, power and dc sources. The dc source here, in our case, is SPV with a capacitor. In this system, a filter is needed as the interface between the inverter and the MHP. The LCL filter has been modeled and the parameter has been calculated based on (Ruan et al., 2018) to provide smooth current injection. Compared with the L filter, the LCL filter is consi dered a preferred choice for its costeffective attenuation of switching frequency harmonics in the injected grid currents (Ruan et al., 2018). While integrating synchronverters with other resources, synchronization is an important phenomenon. Among various synchronization techniques, one of the wellknown

and popularly used control technique for power systems is synchronous reference frame Pha se Locked Loop (PLL) (Kathiresan et al., 2020) that is used to synchronize the SV to MHP in this study.

The modelling of SV is based on the mathematical equations where equations for voltage sig nal and power are shown below:

$$e = \dot{\theta}\, M_f i_f \widetilde{sin\theta} \quad (16)$$

$$P = \dot{\theta}\, M_f i_f\, i, \widetilde{sin\theta} \quad (17)$$

$$Q = \dot{\theta}\, M_f i_f\, i, \widetilde{cos\theta} \quad (18)$$

Where e the three-phase reference signal given to the pulse width modulation (PWM) generator and P is the electrical power developed by the SV. The generated $e_a, e_b and\ e_c$ are given to PWM generator of three phase inverters. $M_f and\ i_f$ are the maximum mutual inductancebetweenthe stator winding and the field winding and field excitation current. The field winding and field excitation current here mentioned is a fictious as this generator mimics the synchronous machine. Similarly, i is the stator phasor current in three-phase and phasor sine is defined given by equation 3.

$$\widetilde{sin\theta} = [sin\theta, \sin\left(\theta - \tfrac{2\pi}{3}\right), \sin(\theta + \tfrac{2\pi}{3})]$$

The $M_f i_f$ is determined using the following equation:

$$\dot{M_f I_f} = \tfrac{1}{K}((v_m - v_{ref})D_q - Q) \quad (19)$$

The rotor dynamic equation that is imitated by the SV is given as:

$$\ddot{\theta} = \tfrac{1}{J}(T_m - T_e) \quad (20)$$

Where J is the virtual inertia of the SV,

Tm, is the fictitious mechanical torque developed, Te is the electrical power developed and D p is the droop regulation parameter. Similarly, θ is the virtual power angle of the SV, which c an be artificially regulated or reset using signal processes while synchronization and power sharing. The peak voltage is calculated as:

$$v_m = \tfrac{2}{3}\sqrt{-(V_a V_b + V_b V_c + V_a V_c)}$$

Where, $V_a, V_b \; and \; V_c$ are line voltages measured by voltage sensors. The parameters for the virtual synchronous machine used in the analysis has been approximated and calculated based on reference (Zhong et al., 2010). The equation has been solved using the MATLAB/SIMULINK function block. The reference signal generated is compared with a triangular pulse signal of 5 kHz frequency to generate gate pulses for the switching circuit of the inverter.

3.2.1.2.Modelling of Solar PV

The mathematical model for solar PV is adapted from (Allani et al., 2018) using the simplified equivalent circuit for the real and practical case as shown in Figure 2. The PV Array block uses a five-parameter model using a light-generated current source (IL), diode, series resistance (Rs), and shunt resistance (Rsh) to represent the irradiance- and temperature-dependent I-V characteristics of the modules. 10.66 kW rating of solar PV using the preset 1STH-215P PV module model from the National Renewable Energy Laboratory (NREL) System Advisor Model (2018) has been used in the simulation. The equation for PV current for the cell is given as:

The voltage current characteristic equation of a solar cell is obtained from(Salmi et al., 2012; Tsai et al., 2008). The module photo current I_ph is given as:

$$I_{ph} = [I_{sc} + K_i(T - 298)] \times I_r/1000 \qquad (21)$$

Here, Iph: photo-current (A); Isc: short circuit current (A) ; Ki: short-circuit current of cell at 25 °C and 1000 W/m2; T: operating temperature (K); Ir: solar irradiation (W/m2).

The module reverse current is given as:

$$I_{rs} = I_{sc}/[\exp\left(\frac{qV_{OC}}{N_s knT}\right) - 1]$$

Here, q: electron charge, = 1.6 × 10−19C; Voc: open circuit voltage (V); Ns: number of cells connected in series; n: the ideality factor of the diode; k: Boltzmann's constant, = 1.3805 × 10−23 J/K.

The module saturation currents I_o varies with the cell temperature which is given by:

$$I_0 = I_{rs}\left[\frac{T}{T_r}\right]^3 \exp\left[q \times \frac{E_{g0}}{nk}\left(\frac{1}{T} - \frac{1}{T_r}\right)\right]$$

Here, Tr: nominal temperature = 298.15 K; Eg0: band gap energy of the semiconductor, = 1.1 eV; The current output of PV module is:

$$I = N_p I_{ph} - \mathrm{N_p} \times \mathrm{I_0} \left[\exp\left(\frac{\frac{V}{N_s} + \mathrm{I} \times R_s / N_p}{n \times V_t}\right) - 1\right] - I_{sh}$$

$$I_{sh} = (V \times \frac{N_p}{N_s} + I \times R_s)/R_{sh}$$

$$V_t = k \times \frac{T}{q}$$

Here: Np: number of PV modules connected in parallel; Rs: series resistance (Ω); Rsh: shunt resistance (Ω); Vt: diode thermal voltage (V).

The current -Voltage and Power -Voltage Characteristics of the Solar PV is shown below:

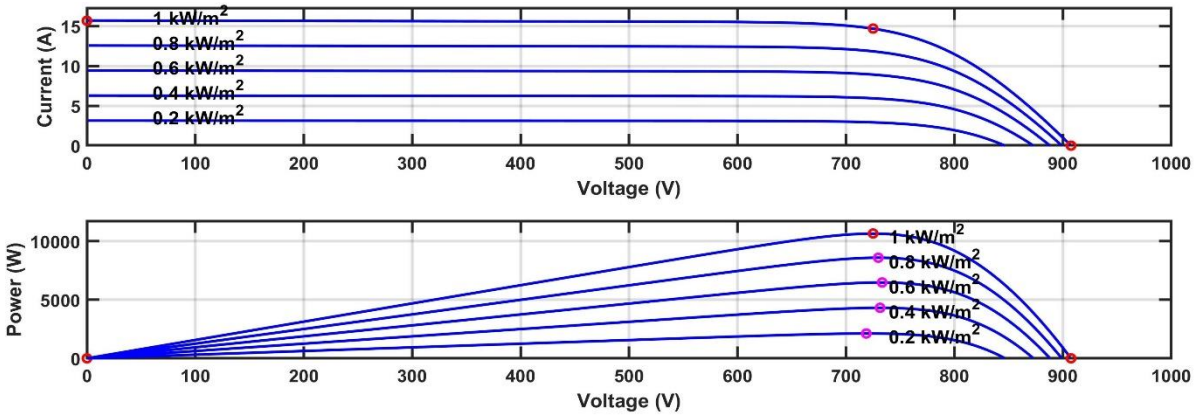

Figure 7: Current - Voltage and Power - Voltage Characteristics of the solar PV of rating 1.1 kW taken in the study.

3.2.1.3.Modelling of MHP

The MHP has been realized using the models of major components such as hydraulic turbines, synchronous machine, excitation system, and electronic load controller. The synchronous generator has some advantages over the induction generator for such systems. Synchronous generators can run isolated from the grid and they can produce power since excitation is grid independent (B. Singh et al., 2008). Also, synchronous generators 5 are readily available in the market, no excitation capacitors are required to provide reactive power. Highly efficient synchronous generators have inbuilt AVR for voltage regulation and using a synchronous generator with ELC one can achieve good frequency regulation.

The standard model of synchronous generator in d-q frame of reference can be written as:

Differential Equations:

$$\frac{T'_{do}dE'_q}{dt} = -E'_q - (X_d - X'_d)I_d + E\_fd$$

$$\frac{T'_{qo}dE'_d}{dt} = -E'_d - \left(X_q - X'_q\right)I_q$$

$$\frac{d\delta}{dt} = \Delta\omega$$

$$\frac{Jd\Delta\omega}{dt} = P_m - P_{ei} - D\Delta\omega$$

The terminal voltage in dq frame of the synchronous machine can be written as:

$$v_d = E'_d - R_{sg}I_d - I_qX'_q$$

$$v_q = E'_q + I_dX'_d - I_qR_{sg}$$

Among the several models of synchronous machine, the IEEE standard 1110-2002 ("IEEE Guide for Synchronous Generator Modeling Practices and Parameter Verification with Applications in Power System Stability Analyses," 2020) using the preset model of SIMULINK has been used in the simulation. The rating of preset 8.1 kVA,50 Hz,1500 rpm,400 V salient pole synchronous machine has been used. The excitation system block is a Simulink system implementing a DC exciter described in (Group et al., 1992), without the exciter's saturation function. The basic elements that form the excitation system block are the voltage regulator and the exciter. A constant reference voltage of 1 per unit(400 V) is given as a reference voltage signal for the excitation system. Hence, this does not consider the voltage drop on the load side of the system. The generalized equation of the excitation system is given below:

$$\frac{T_AdE_{fd}}{dt} = -E_{fd} + K_A(v_{ref} - v_t)$$

Where, E_{fd} is the field excitation voltage, $K_A and\ T_A$ are the exciter gain and time constant. $v_{ref}\ and\ v_t$ are the reference voltage and terminal voltage of the synchronous machine. The terminal voltage is calculated as:

$$v_t = \sqrt{v_d^2 + v_q^2}$$

Similarly, hydraulic turbine block implements a nonlinear hydraulic turbine model as described in (Mover et al., 1992).

Additionally, the model done in dq frame is converted to abc frame using park transformation which is given as:

$$V_{dq0} = P \times V_{abc}$$

In reverse,

$$V_{abc} = P^{-1} V_{dq0}$$

$$P = \begin{bmatrix} cos\theta & \sin\theta & 1 \\ \cos(\theta - \frac{2\pi}{3}) & \sin(\theta - \frac{2\pi}{3}) & 1 \\ \cos(\theta + \frac{2\pi}{3}) & \sin(\theta + \frac{2\pi}{3}) & 1 \end{bmatrix}$$

Similarly, the current can also be converted in abc frame of reference.

$$I_{dq0} = P \times I_{abc}$$

$$I_{abc} = P^{-1} I_{dq0}$$

The mathematical model of power part of the synchronverter is given below:

$$\frac{m_d V_{dc}}{2} = \frac{L_f di_{d,inv}}{dt} - \omega_s L_f i_{q,inv} + R_f i_{d,inv} + V_{d,inv}$$

$$\frac{m_d V_{dc}}{2} = \frac{L_f di_{q,inv}}{dt} - \omega_s L_f i_{d,inv} + R_f i_{q,inv} + V_{q,inv}$$

$$\frac{C_{dc} dV_{dc}}{dt} = \frac{P_{pv} - P_{vsc}}{V_{dc}}$$

$$P_{vsc} = \frac{(m_d V_{dc} i_{d,inv} + m_q V_{dc} i_{q,inv})}{2}$$

Where, $m_d and\, m_q$ are the duty cycle of the synchronverter. The duty cycle is generated by the pulse width modulated signal generator. The model of duty cycle is approximated with first order model as.

$$T_d \frac{dm_d}{dt} = -m_d + k_d E_{ref}$$

3.2.1.4.Modelling of Electronic Load Controller (ELC)

In this study, an electronic load converter is realized using a three-phase diode bridge rectifier to provide dc power regulation for ballast load. Speed regulation control strategy is obtained by taking the speed error and providing an appropriate duty cycle through Proportionate, Integral and Derivative (PID) controller to Pulse Width Modulation (PWM) generator. The equation for duty cycle is given below:

$$\alpha = \Delta\omega(K_p + \frac{K_i}{s} + sK_d)$$

The Mathematical model for ELC current is taken as:

$$T_{inv}\frac{dI_{elc}}{dt} = -I_{elc} + \frac{V_{ts}}{R\_ballast}\alpha$$

The PWM generator would turn on the transistor for the time of duty cycle to regulate the power transfer ballast resistor. The variation of the load will compensate by the loading in the ballast load. The model has been adapted from reference (Rai et al., 2015) and shown in Figure 6 4. Sinusoidal voltage wave forms are chopped when the antiparallel connected thyristors are fired. Due to chopping, the dump load through resistive draws lagging current. The synchronous generator provides the reactive power demanded by the dump load. An appropriate LCL filter circuit has been provided to reduce the voltage harmonics. The parameters for the LCL filter for harmonic reduction and smooth current injection are calculated based on reference (Ruan et al., 2018).

3.2.1.5.Modelling of Load

Generally, the electricity consumption in rural areas is contributed by lighting and milling requirements. Hence, this study has considered two loading conditions. We have used the balanced variable three-phase resistive load to mimic the lighting load in one situation. While, in another case, we have implemented induction motor load to represent the milling load requirement. The load is assumed to draw only the active load during the resistive and partially reactive loads during the induction motor. The resistive load has been varied by connecting several resistive load blocks at different simulation times. Similarly, load torque has been changed at other simulation times for induction motor load. For induction motor load, a model of squirrel case induction motor from SimPower library of Simulink of rating 4 kW,400 V, 1430 RPM has been used in the study.

Mathematical expression of impedance type of load in dq frame of reference:

$$Z_{load} = R_{load} + jX_{load}$$

$$V_{load} = i_{load} \times Z_{load}$$

$$i_{load} = i_{d,load} + ji_{q,load}$$

$$V_{load} = V_{d,load} + j\,V_{q,load}$$

3.2.2. Load Sharing and Control Strategy

The power transfer from SV and MHP can be done by controlling the load angle between the inverter and MHP. The load sharing and control operation is performed using the technique of power angle control(PAC) method adapted from (Elsavad et al., 2017; Svensson, 1995; Vijayakumari et al., 2016). Moreover, the maximum power from the SPV can be extracted using the phase angle control (Menon, 2016). Initially, the solar and MHP are synchronized at a simulation time of 0.5 second by obtaining the phase angle of MHP output voltage θg via. phase lock loop (PLL) control system. The power-sharing mechanism is performed by varying the power angle(δ) between the MHP and inverter output voltages. During synchronization, the inverter voltage θ is reset to θg − δ. This will result in the power transfer from the synchronverter to the MHP to be:

$$P = \frac{V_{inv}\,V_{mhp}}{X}\sin(\,\delta_{inv} - \delta_{mhp}$$

$$= \frac{V_{inv}V_{mhp}}{X}\sin\big(\theta - \theta_{mhp}\big) \approx \frac{V^2}{X}\sin\,(\Delta\delta)$$

Where, $\theta_{mhp} = \omega_{mhp}t$ is the measured by PLL and Vinv and Vmhp are the syncronverter and micro-hydro voltages. The power flow between the converter and MHP is controlled by resetting the θ angle of the VSM as shown in the detailed figure, with the following angle defined by the droop equation. Using the power and droop control equation(Majumder et al., 2009), the change in power angle to share power between SPV and MHP can be written as follows:

$$\Delta\delta = \beta \times (P - P_{rated})$$

Where, P is the power set which is proportional to the irradiance level of the Solar PV. Hence, the equation for change in angle can be written as:

$$\Delta\delta = \beta \times (n \times I_{rr} - P_{rated}) = \gamma \times I_{rr} - \beta \times P_{sv,rated}$$

Where α and γ depend on the rating of the Solar PV panel, and Irr is the irradiance level. Prated is the maximum power that can be generated by solar PV at 1000 W/m2 irradiance level. The constant δ angle maintained between the SV and MHP as per the irradiance level will result in the power flow from SPV to MHP similar to load sharing that of a parallel synchronous machine. During isolated MHP operation conditions, all load is handled by MHP. The dynamic load variation is dealt with by ELC. Load sharing is predominantly by solar PV during day conditions, and only during the excess power need condition will the MHP share the appropriate load.

3.2.3. Detail Simulation and Analysis

A proposed micro-grid system depicted in figure 6 has been implemented in Matlab/Simulink 2018b platform with Simscape Electrical to demonstrate the effective power-sharing between the sources. The simulation is performed using an ode23tb(stiff/TR-BDF2) solver with a step size of 1e-6. The circuit breaker on the syncronverter side is used to disconnect the inverter system when the irradiance level is too low to protect the system from a reverse power supply. Similarly, a circuit breaker on the MHP side is used for initial synchronization in the simulation process. The signal in the circuit breaker is made to operate to disconnect when the irradiance level is too low (less than 100 w/m2 used in the study). The breaker will be instantly closed when the irradiance level rises. The re-closing of the circuit breaker does not affect the re-synchronization as the inverter output voltage is reset in every sampling time with the value calculated using equation 10. Voltage and current measurement blocks are used to measure the instantaneous voltage and current at the source terminals. The active power has been calculated using the measured instantaneous voltage and current. Since the ballast load lies under the MHP block, during the low loading condition, when the SV can only supply the load, the ballast load has to consume the excess power from the solar PV with sum to the rated capacity of MHP (from the electronic load converter). The overall model layout for the hybrid system is shown in Figure 1.

CHAPTER FOUR: RESULTS

4.1.Optimal Sizing of Solar PV- MHP Hybrid System

4.1.1. Optimization Results

The system optimal net present cost trend versus iteration number of different algorithms for the two-hybrid systems is illustrated in figure 8. As we have used the stochastic-based derivative-free algorithm, the optimal solution varies for each algorithm's execution. The variation of the optimal net present cost of the system for different 30 executions is shown in figure 9. Among the three algorithms, the artificial bee colony optimization algorithm seems to have the least standard deviation with the best least solution. In contrast, the genetic algorithm appears to have the worst performance. The optimal net present cost for storage and the non-storage-based system is found to be about 96,740 USD and 86,310 USD, respectively. The optimal design discharge for the MHP comes to 0.121 m3/sec and 0.173 m3/sec and design gross head of 39.62 m and 39.8 m, which is near the maximum limiting value for storage and non-storage system, respectively. Similarly, results of optimal cost and capacities of components for the proposed hybrid system with storage and non-storage based obtained from artificial bee colony algorithm are listed in table 1.

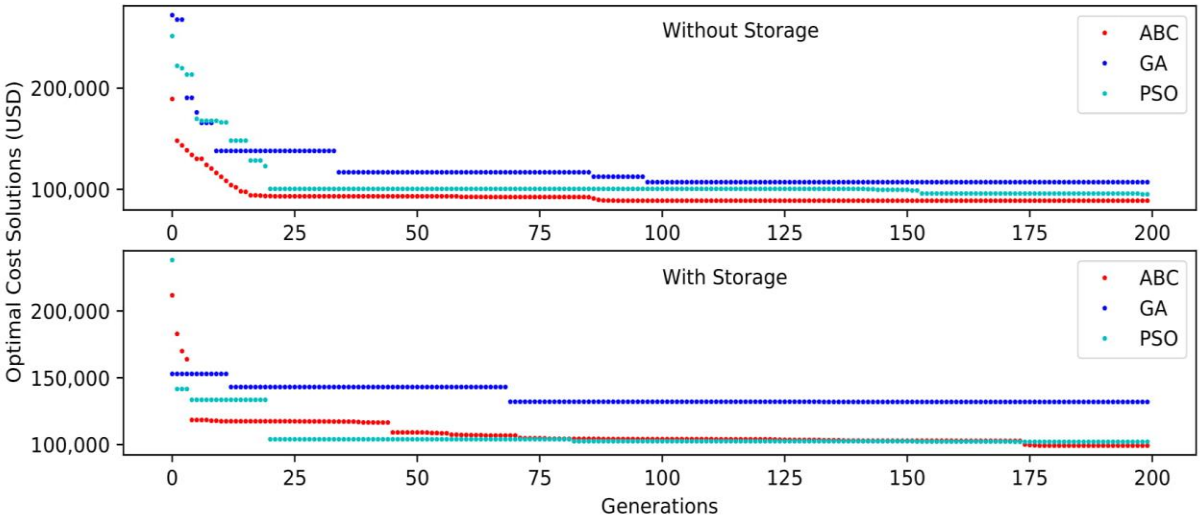

Figure 8: Optimal solution in different iteration for different algorithms for storage and without storage cases.

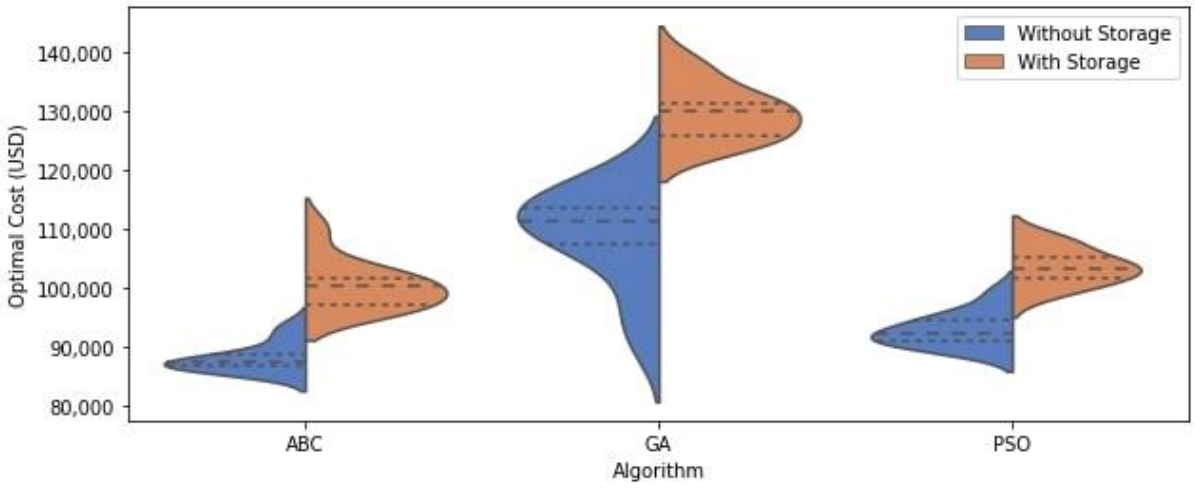

Figure 9: Optimal cost distribution generated for multiple algorithm.

Table 1: Result of optimization from Artificial Bee Colony algorithm. The total size of the system is relatively greater in a system that does not have storage.

	With Storage					**Without Storage**		
	SPV	MHP	Battery	Inverter	Total	SPV	MHP	Total
Optimal Size(kW)	12.2	23.5	25.8	12.6	35.7	3.7	33.8	37.5
Investment Cost (USD)	8,302.80	41,812.00	5,156.00	2,512.00	57,782.80	2,523.50	60,126.50	62,650.00
Operation and maintenance cost (USD/annum)	122.1	2,090.60	-	-	2,212.70	37.1	3,006.30	3,043.40
Replacement cost (USD)	-	-	5,156.00	2,512.00	7,668.00	-	-	-

The power generation varies as per the variation of resource parameters such as discharge in-stream and irradiance level throughout the year. Similarly, the consumption pattern varies with days but is assumed to be similar for every week, as mentioned before. During the wet season, MHP generates almost constant power, which could be sufficient for the load supply. But during the dry season, the variation of river flow results in the load outage for the non-storage-based hybrid system as can be seen in figure 10 shows the load sharing and consumption pattern for a typical week of month April. The number of outages that occur lies in this season due to insufficiency of generation. The negative values in the power of the electronic load converter in Figure 10 show the amount of energy-deficient in the system during the time. As already mentioned, for non-storage, the total outage numbers have been limited to 200 hours. Only about 860 kWh of energy was found to be deficient in the system for the whole year. With the

total consumption of about 148,984 kWh of electricity for a year, about 140,00 kWh of energy dissipated in ELC. Hence, appropriate demand-side management or an appropriate storage mechanism can be done to minimize the total size of the system and outage. Additionally, with grid availability, the amount of power dissipated in ELC can be supplied to the grid.

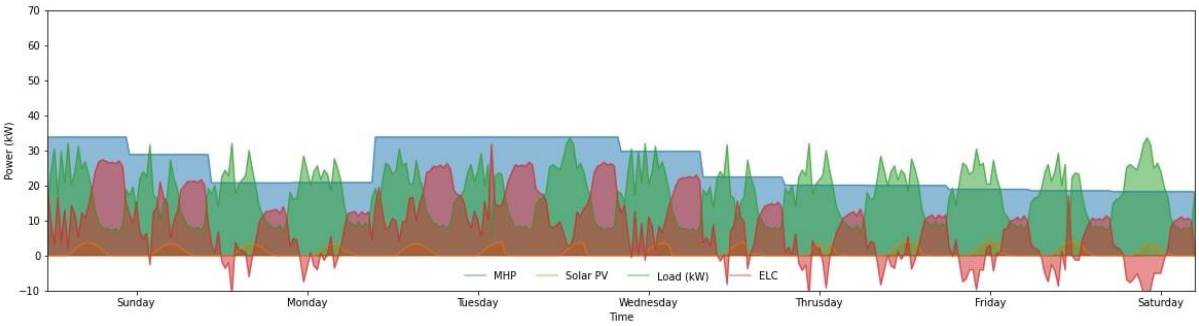

Figure 10: Power sharing between solar PV and MHP with load and power dissipation on ELC.

An appropriate storage unit in the system stores the excess power generated, which removes the number of outages in the season (Figure 9). Further, it even reduces the total sizing of the hybrid system (Table 1). The load sharing by hybrid components in the typical dry season, i.e., the week of April, is shown in Figure 10. Which ultimately removes the outages in the system throughout the year.

The state of charge of the storage system is within the range of constraint as defined. The storage system seems to be discharged highly on Saturday, as the day possesses maximum load demand compared to other days.

Throughout the year, about 85 % of the time, the state of charge of the battery system remains more significant than 0.9. The total power dissipated in the ELC for the whole year is found to be about 69,874 kWh which is more than half as in the case of the non-storage-based hybrid system.

As the use of storage results in no outage in the system, the storage-based system does not provide any outages. The total energy supplied to load for the whole year is found to be about

154,220 kWh which is almost about 3.5 % greater in the case of the non-storage-based system.

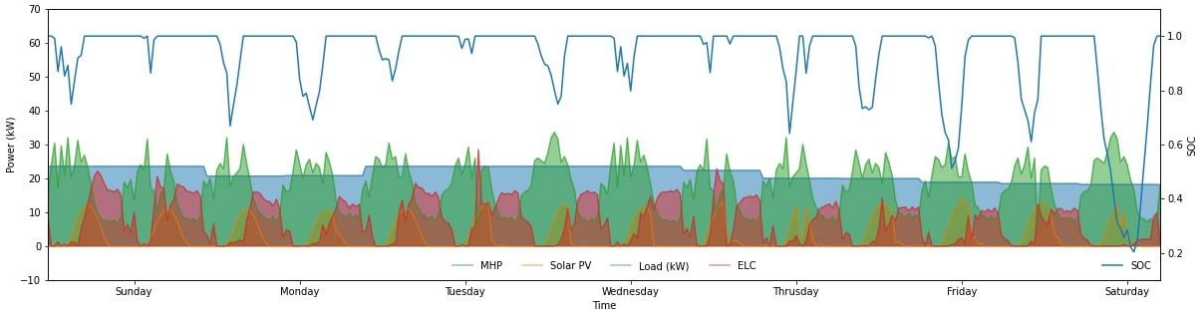

Figure 11: Load sharing between solar PV and MHP in typical dry month with loading, ELC power and battery State of Charge

4.1.2. Financial Analysis

The total initial investment, annual revenue (selling the electricity to residential area), and operational and maintenance cost with replacement cost (in case of Storage one) are shown in the cash flow diagram in figure 12. The cash-flow diagram for both storage-based and non-storage-based systems has been compared. The initial negative value on the cash flow diagram shows the investment of the system, while the later on value is the difference between revenue and maintenance with replacement cost. The discounted payback period for both of the system non-storage exceeds the project life. This is mainly due to the value of the discount rate, which is generally affected by the country's economics, taken in the study. Taking the discount rate of 7 percent would result in the discounted payback period of 15 and 18 years for the storage-based and non-storage systems, respectively. The Internal rate of return for storage and without a storage-based system comes with 9.8 % and 8.6 % for the base values taken into consideration. Each four-year and ten-year replacement cost for battery and inverter has also affected the NPC of a storage-based system. But its generation revenues are higher due to the availability of energy for all year. In addition, the benefit-cost ratio for a storage-based system comes to be 0.992 and for a non-storage-based system comes to be 0.902. Taking the discount rate of 7 percent would result in the BCR ratio of 1.152 and 1.257 for without storage and with a storage system. The BCR is relatively lesser in storage system than without storage one resulting in the greater financial viability of storage based one. Moreover, the economic consideration of social benefits has not been considered in the BCR ratio analysis.

Similarly, The LCOE for Storage and not storage is obtained 0.067 USD/kWh and 0.072 USD/kWh, respectively. This shows the storage-based system is relatively cheaper than non-storage based in SPV- MHP hybrid system. This is due to the oversizing of system components to fulfill the constraint of ELF in a non-storage-based system.

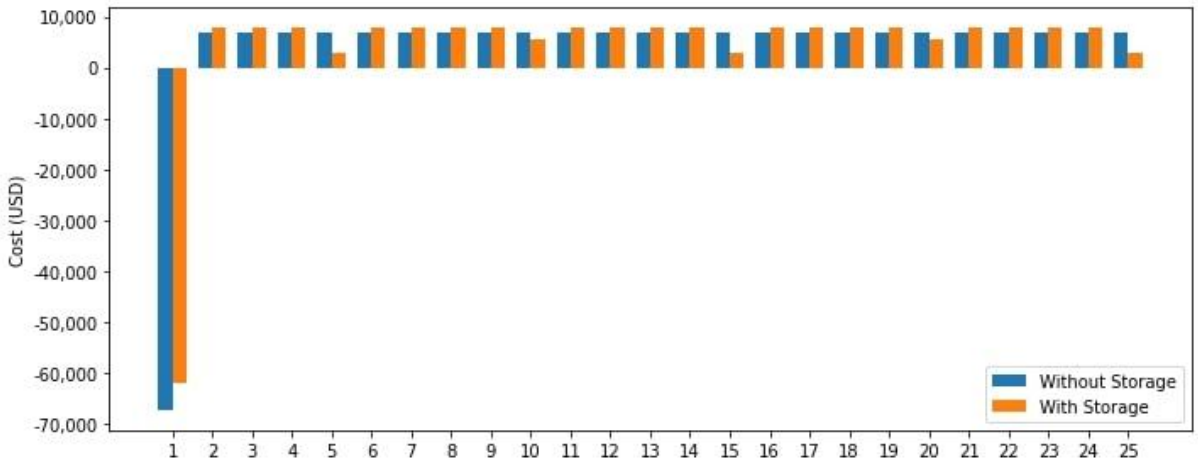

Figure 12: Cash flow diagram of the storage and non-storage based SPV-MHP system for project lifetime.

4.1.3. Generation Uncertainty Analysis

In the uncertainty analysis, the GHI data is fitted for the probability distributions with lognormal, beta, and gamma distributions, as shown in figure 8 left. The Chi-square value of each of the distributions, beta of 101.992, lognormal of 2,136.798, and gamma of 3,277.618, has been determined. Based on the least chi-square, beta distribution has been chosen for Monte Carlo simulation. The distribution fitting for each of the distributions is shown in figure 8 (a). The different yearly data (for daylight conditions) has been generated randomly using the beta distribution. For each of the annual data generated, optimization is performed. The optimization is performed for several randomly generated yearly GHI data. The normalized sizing capacities distribution and net present cost distribution obtained on each optimization result of randomly generated yearly GHI data are shown in Figure 8 right for both systems. The uncertainty of the solar GHI has more effect on the storage-based system rather than the non-storage one, as can be seen in figure 8 (b). The mean for SPV, MHP, and cost for non-storage is about 11.7 kW, 33.9 kW, 100,360 USD with a standard deviation of 2.5 kW, 0.48 kW 5894.7 USD, respectively.

Similarly, for the storage-based hybrid system, the mean for SPV, MHP, storage size, and cost are found to be about 22.98 kW, 21.77 kW, 40.53 N, 120,338 USD with a standard deviation of 8.5 kW, 1.26 kW, 8.61 N, 6,343.86 USD. This uncertainty involves the uncertainty on determining the optimal value in each complete solution, i.e., the uncertainty of the algorithm as previously shown in figure 4. In addition, the average optimal cost of the uncertainty of the system is found to be 11.2 % and 12.4 % of that of certainty case (sub-sec. 3.2) for non-storage and storage-based systems, respectively.

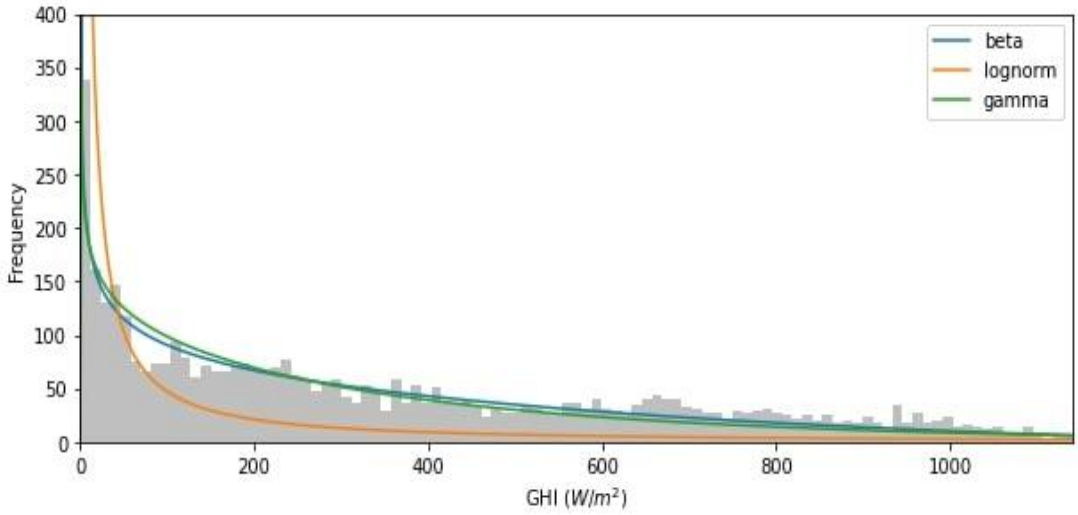

Figure 13: Probability distribution fitting of solar irradiance data in Beta, Lognormal and gamma distribution.

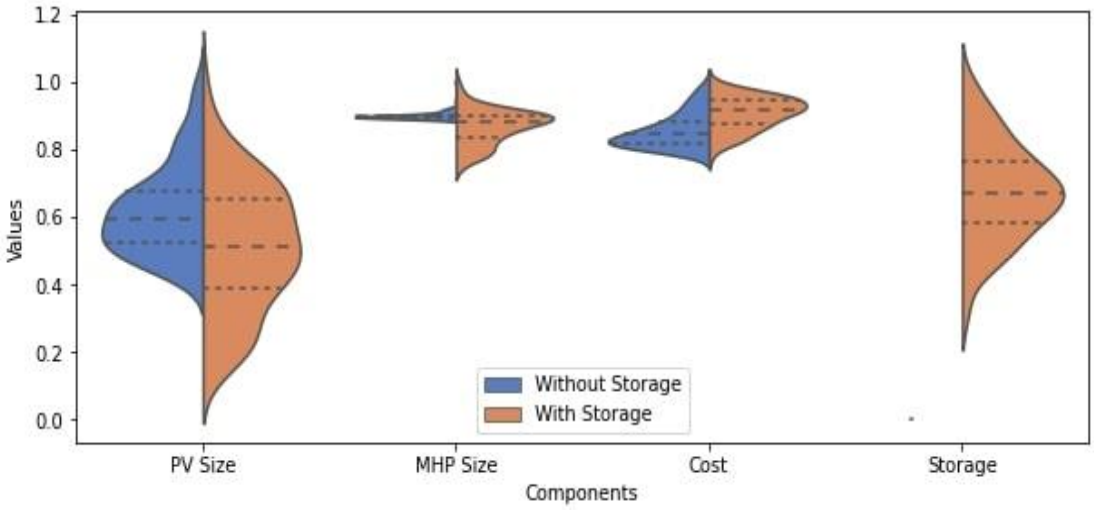

Figure 14: Variation of sizing of components with cost due to irradiance uncertainty.

4.1.4. Cost of Outage

Due to the outage in the case of without storage-based system contributes the additional cost in the system called as cost of outage. As the storage-based system possess no outages, the difference in the total energy provided by storage based minus the total energy provided by without storage-based system give the outage energy. From the analysis the outage energy is found to be 860 kWh. Using the tariff rate in the analysis the total cost of outage is found to be 62.78 USD. This cost of outage still discourages the use of without-storage based system. However, this outages can also be positively treat for the maintenance purpose of the hybrid system.

4.1.5. Sensitivity Analysis

In sensitivity analysis, the LCOE for the hybrid system for different parametric values for both systems has been shown in figure 7 (a). The LCOE of the system seems to be highly dependent on the investment cost of MHP and the interest rate. The LCOE for different equivalent loss of load factors has also been shown for both storage and the non-storage-based hybrid system in figure 7 (b). Since the size of SPV decreases with the increment of outage rates in a year, the LCOE seems to decline for more excellent outage rates. The optimization process for the non-storage-based hybrid system does not converge for outage rates of less than 170 outages per year. This is because of the unavailability of SPV after daylight conditions and the insufficiency of MHP power for the load during the dry season. The cost highly escalates for the lower level of outages for non-storage ones. In the case of Storage one, the cost remains almost steady for different outages scenarios too.

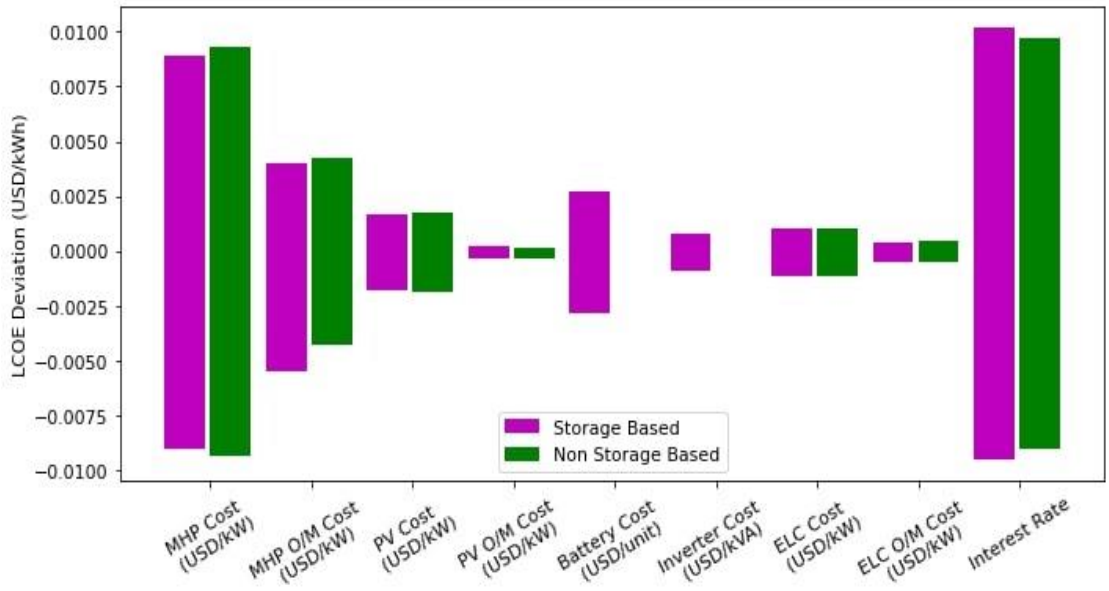

Figure 15: Sensitivity of LCOE with several parameters of the hybrid system.

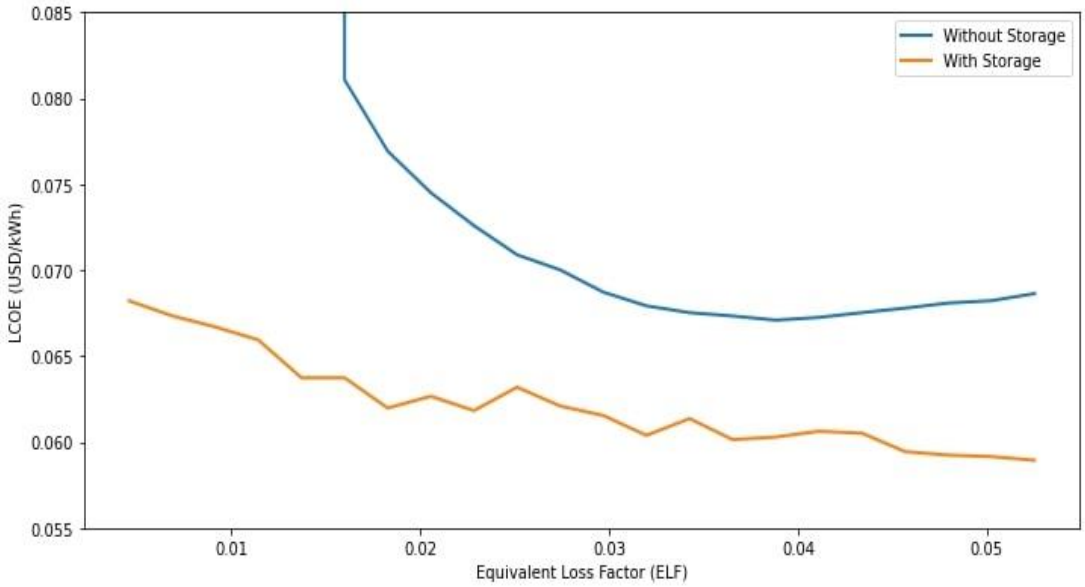

Figure 16: Variation of LCOE with different loss of load factor.

4.2.Performance Analysis of Hybrid System

Before synchronization with MHP, SV virtual angle (θ) is reset to the reference voltage angle of MHP measured by PLL with added load angle as explained in section 3 at simulation time of 0.35 sec that causes a slight voltage, current, and frequency distortion in the system at the time. The actual power generated by the syncronverter will be the sum of losses in the line and power shared to load and the excess power lost in the ballast load. As the measurement block for the SV side is kept after the line, the actual power generated by the SV is the sum of total line losses from SV and the measured value. The Total Harmonic Distortion (THD) of the load current and voltage has been measured.

The value of parameters used in the simulation is shown in Table 2:

Table 0-2: Parameters used in the simulation of the hybrid system.

Parameter	**Value**	**Parameter**	**Value**	**Parameter**	**Value**
Rated Voltage (base V), V s	400 V	SV Reactive power droop g ain, K	500	Filter Inductance, Ls	10mH
Rated Inverter power, Si	12 kV A	Rated solar pv, PP V	10.01 k W	Filter Capacitence, Cs	0.5 uF
Switching Frequency, fs	5 kHz	Voltage Reference, Vref	1 pu	Line Resistance, Rg	1 Ω
SV Inertial Constant, J	2	Speed Reference, ωref	1 pu	Line Inductance, Lg	0.025 H
SV Damping Coefficent, D	636	Turbine Gain, k	1 pu	Ballast Load Resistance, Rb	10 Ω

SV Voltage Droop Coefficient, K	0.6437	Water Time constant, Tw	1 sec	Alternator Rating (Base kVA), SA	8.1 kVA
Reference Power, Pref	1 pu	Turbine Damping Coefficient, βt,	1 pu	System Frequency, f	50 Hz
PV source capacitance, CPV	500 uF	PV source Resistance	0.5 Ω	Solar DC Max Voltage, VPV	900 V
Exciter Gain, Ke	300	Exciter Time Constant, Te	0.001	Sample time Ts	1 us
δ Control Parameter, K	10	δ Control Parameter, β	-0.0045	Maximum Power SV, Pmax	10.01 kW
ELC Proportionate gain, P	50	ELC Integral gain, I	100	ElC Derivative gain, D	0.05

4.2.1. Standalone MHP Condition

The standalone MHP system consisting of ELC, SG, Excitation system, hydraulic system with loading is simulated to verify the SG system with ELC model. Figure 17 shows the power supplied by MHP to load and ballast power. The ELC has provided appropriate load sharing to maintain the system frequency shown in figure 18. The system's frequency seems to be oscillating for a short period during the change in load. The load voltage is slightly below the source or MHP due to the line resistance and reactance. The voltage of the load is decreasing with an increasing load which is shown in 20. The total harmonic distortion of the system is below 5 %, as can be seen in figure 19 besides the condition of transient where the level is THD is too high.

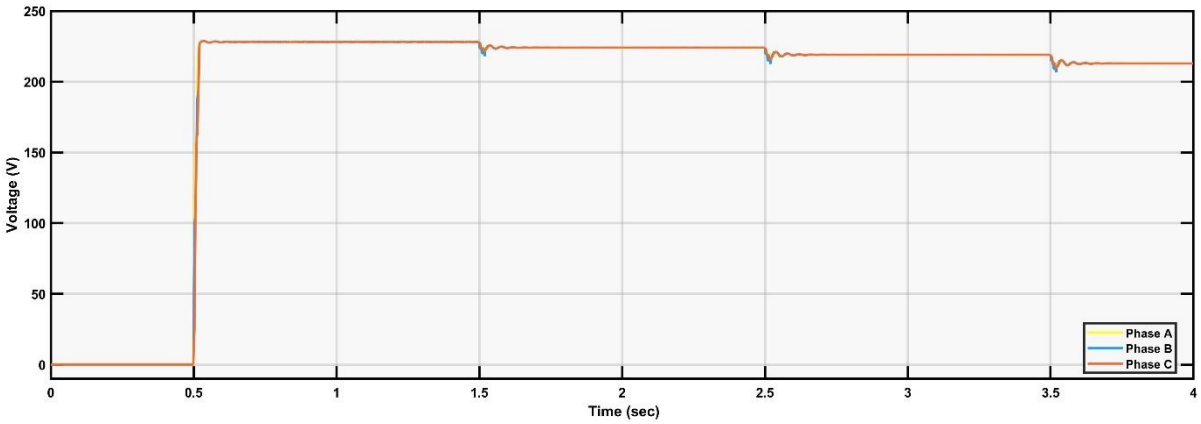

Figure 17: RMS phase voltage profile for different loading condition in standalone MHP condtion.

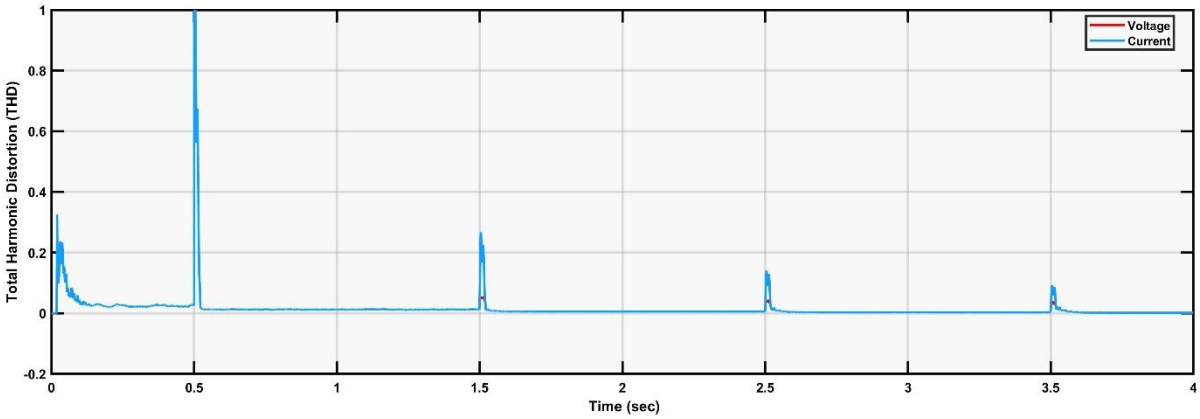

Figure 18: Total Harmonic Distortion (THD) of load voltage during standalone operation of MHP

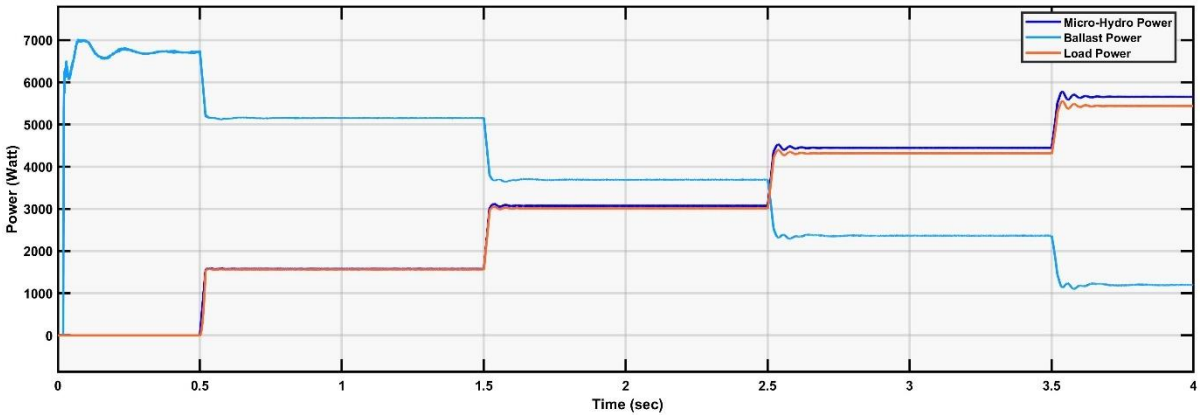

Figure 19: Load sharing of MHP and ELC system during standalone operation

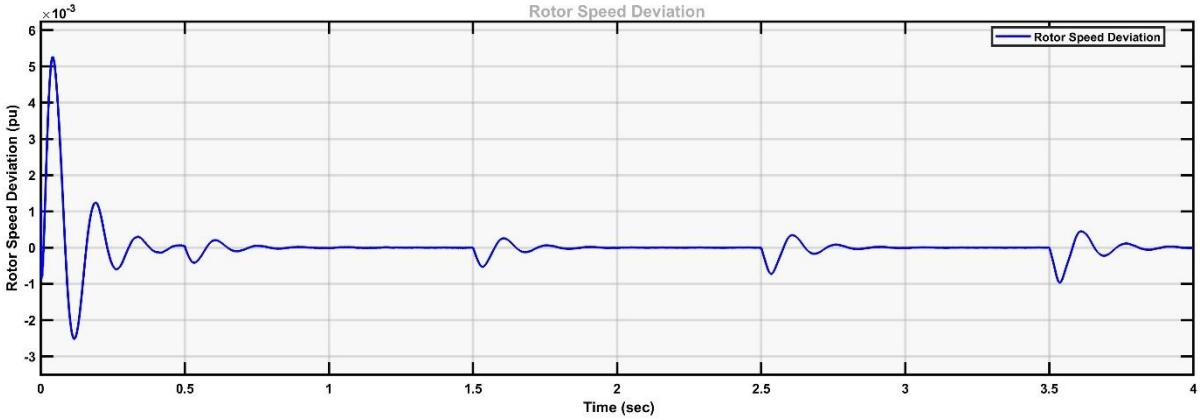

Figure 20: Rotor Speed Deviation during the standalone operation of MHP

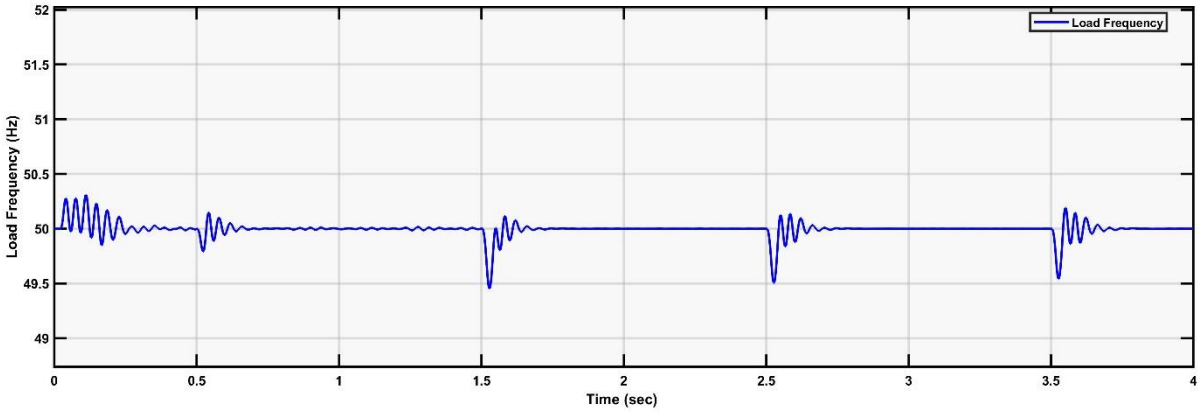

Figure 21: Load frequency variation during the standalone operation of MHP

4.2.1. Constant Irradiance Condition

The simulation is carried out for constant irradiance conditions of 1000 W/m2 and the load is varied. The load used is purely resistive. The load sharing with different loading conditions is shown in the figure 6. Initially, under loading conditions and even when the MHP is not synchronized, the load is supplied by 9 SV only. After synchronization, the excess power generated from SV dissipates to ballast load. The ballast load combined dissipated MHP power and excess SPV power. When the load is increased, the loading is proportionally shared by both of the sources. The SV shares the load until it reaches its rated supply. After a simulation time of 3 seconds, the solar output becomes constant irrelevant to the load increment. After that, MHP will share the load. However, due to the high load and excess current in the line, voltage drop becomes significant. This results in low load power consumption even load is connected. The voltage profile is shown in figure. The simulation has shown that the syncronverter automatically adjusts its power output according to the power requirements. The excess power from solar PV is again dissipated in the ballast load. For low load conditions, the excess power from the syncronverter and MHP cumulatively dissipates into ballast load. This is why the ballast load posses lots of harmonics in light load conditions and smooth power losses in high load conditions. For higher loading conditions, the voltage drop in the load side results in a drop in load power though the load resistive parameter is increased. An appropriate voltage regulation device has to be used to minimize this problem. Moreover, the excitation can be increased by remotely measuring the load voltage or the syncronverter reactive power setting can be adjusted. Sinusoidal voltage and current waveform of load with THD 1.2% has been obtained, which is less than the 5% limit imposed by IEEE519 standard (of Electrical et al., 1981) except during synchronization step load change. The system frequency has not changed by more than ±0.5%. A slight oscillation can be observed during initial load angle

reset, synchronization, and step load variation. Figure 6: Load sharing and voltage profile for different loading level.

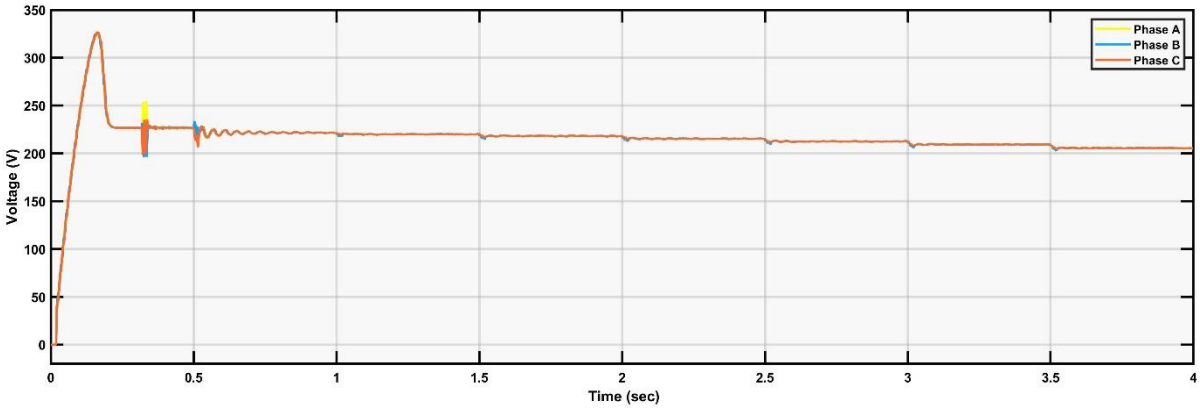

Figure 22: RMS load voltage profile for different loading in hybrid system at constant irridiance.

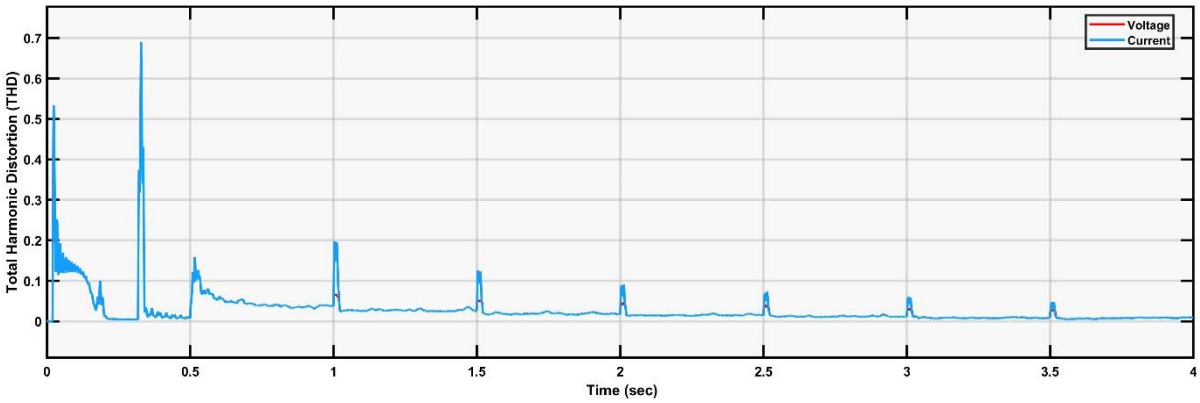

Figure 23: Total Harmonic Distortion of load voltage of the hybrid system for constant irradiance condition.

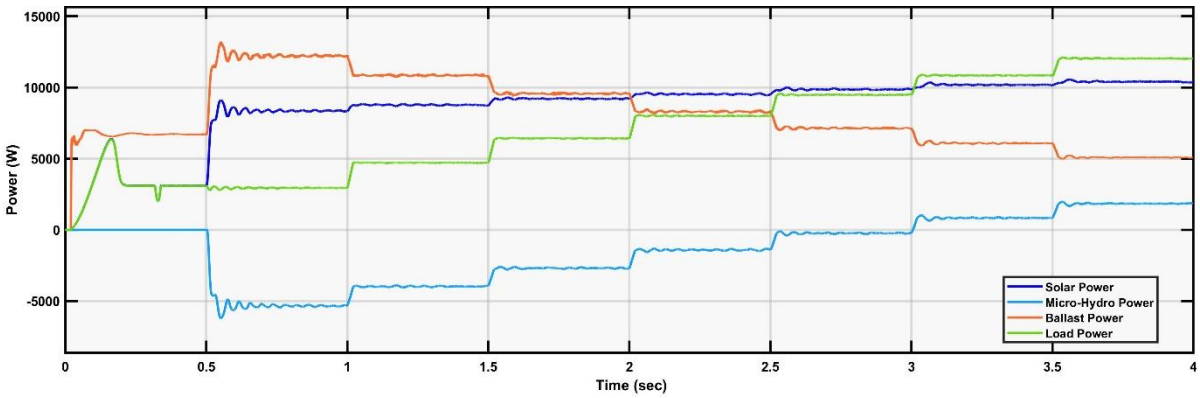

Figure 24: Load sharing by Solar PV, ELC and MHP for constant irradiance condition.

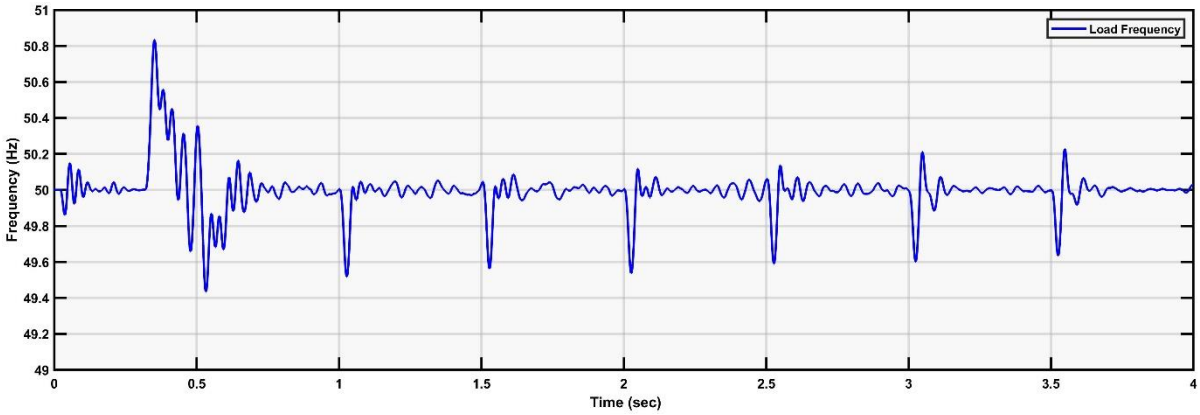

Figure 25: System frequency during load variation in hybrid system at constant irradiance condition.

4.2.2. Effect of Irradiance:

The system is highly affected on the irradiance level which is much unpredictable even in the day time. Hence, the irradiance level is varied to observe the load sharing mechanism in the hybrid system. The irradiance level is reduced from 1000 W/m2 linearly to 500 W/m2 from simulation time 1 to 2 seconds and then left constant. The irradiance again reduced linearly to zero till reaches simulation time 2 and then increased linearly. The load is made constant to 4000 W for all simulation time. As the irradiance level becomes low, the output power from the inverter becomes low which results to take the load by MHP as can be seen in figure 8. Initially, the load is taken by the syncronverter. After synchronization, the excess power from SPV and MHPis dissipated in the ballast load. As the irradiance level becomes low, the output power from the syncronverter becomes low that results in MHP sharing the load to meet the demand. Therefore, during low light or night conditions, the power is solely supplied by MHP. Thus, appropriate scheduling and load shifting have to be done to improve the capacity factor of the hybrid system. The voltage profile has shown a slight oscillation during synchronization but remains constant throughout the simulation time. Hence, the sharing has not affected the voltage regulation of the system. Similarly, the frequency deviation is within the limit of ±0.5%, ignoring the condition during synchronization. When the irradiance level is too low, the SV side gets disconnected from the MHP. This would protect the system from reverse power flow. One of the advantages of using the SV is when the irradiance level is increased that results from the reclose of the circuit breaker, the system will instantly synchronize with the system. During the disconnection of SV, MHP alone has to supply for the whole load that caused the high current to flow and results in a slight voltage drop in the load, which can be mitigated by using appropriate var compensating devices at the load end. The sinusoidal voltage and current waveform with THD 1.3% have been obtained, which is less than 5% limits as mentioned earlier except transient condition as depicted in figure 9.

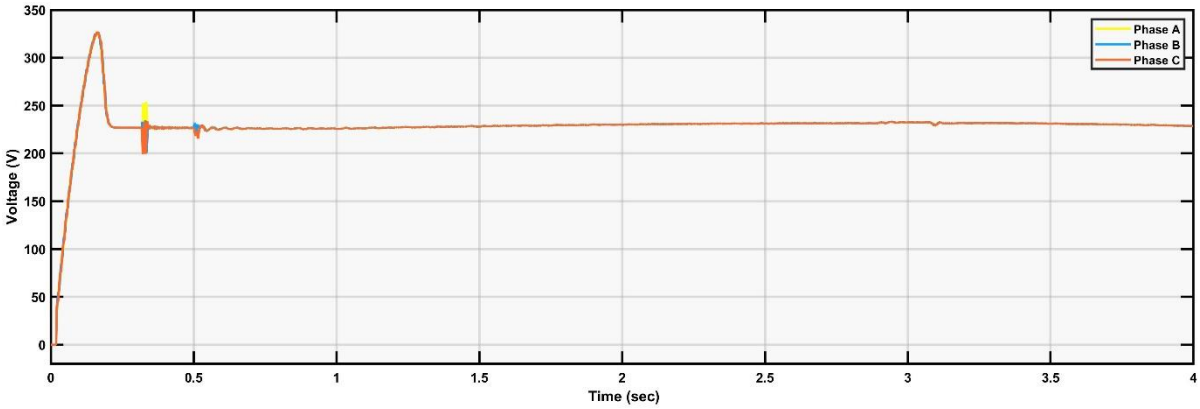

Figure 26: Load RMS voltage profile during the irradiance variation on solar PV.

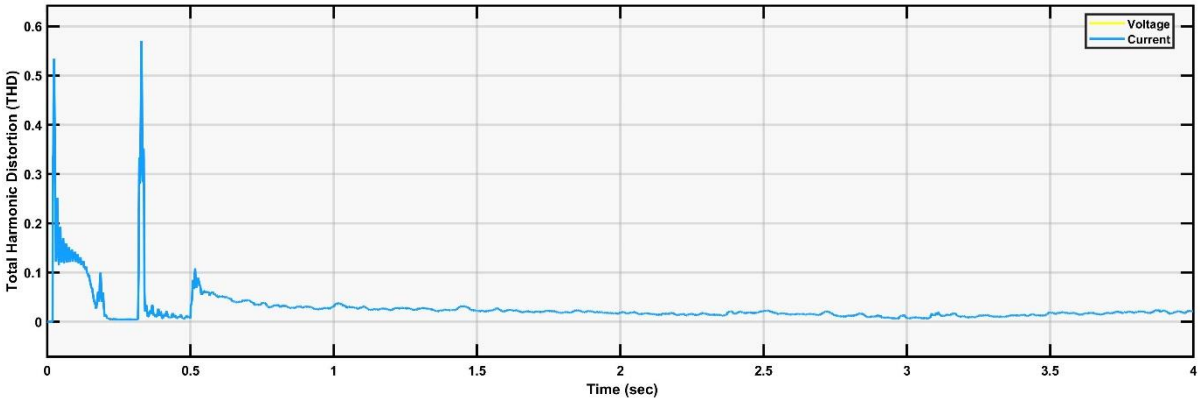

Figure 27: Total harmonic distortion (THD) of the load voltage due to irradiance variation on the hybrid system.

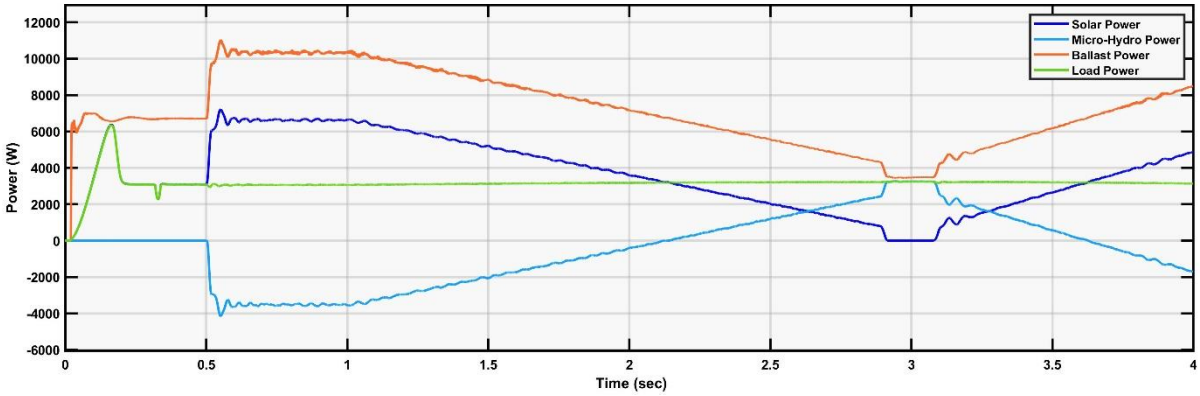

Figure 28: Load sharing by solar PV and MHP during low irradiance in solar PV.

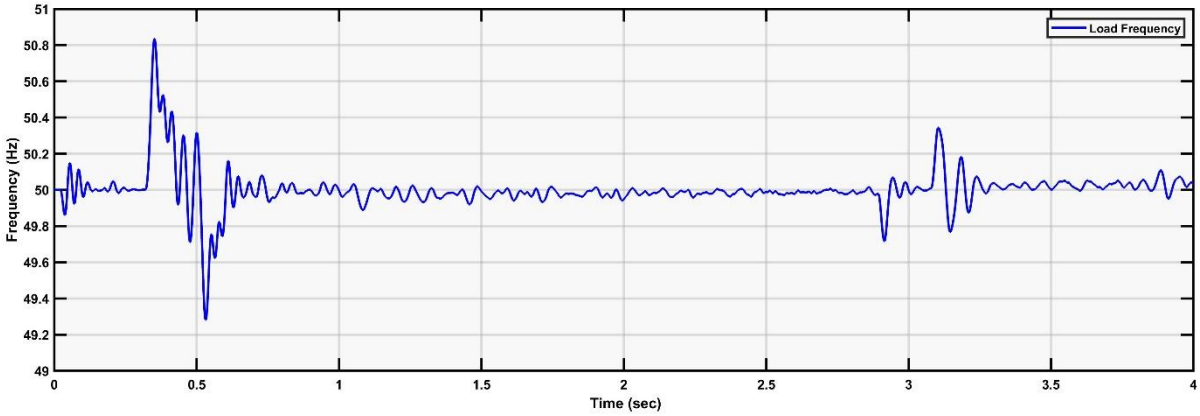

Figure 29: System frequency during the low light and irradiance variation in hybrid system.

4.2.3. Effect of Non-Linear Load:

The simulation is also carried out by using the induction motor as a load. Initially, an induction motor rating 5 kW with zero load torque is taken also with a resistive load of 1500 W. At the simulation time of 2.1 sec, the load torque is increased to full load. To observe the effect of irradiance variation on load sharing, at simulation time 2.6 sec, the irradiance level on SPV is reduced to 800 W/m2(Initially, 1000W.m2). The decrease of irradiance level, reduction of SV output compels the MHP to share the more load as shown in figure 10. The induction motor load torque is again reduced to zero at 3.2sec. The load sharing, voltage profile, and system frequency profile are shown in the figure 10 and figure 11. The application of the induction motor brings the oscillation of system frequency until it reaches to steady-state. Due to the inductive nature of the induction motor, the voltage drop in load is quite high. The increment in motor loading without any var compensating device would lead to voltage instability in the system. The frequency of the system has not deviated more than ±2% ignoring the condition of synchronization. A motor at full load condition draws more resistive current than inductive current resulting in quick damping of oscillation as can be seen in the simulation time interval of 2.10 seconds to 3.25 seconds. Moreover, the load has not been affected by the reduction of irradiance as the supply has been shared by MHP. The sinusoidal voltage and current waveform with THD 1.5% have been obtained, which is less than 5% limits as mentioned earlier subsection. The THD level reduces with the approach of induction motor current/voltage reaching the steady-state level. Moreover, the THD level of current and voltage depends on the level of load shared by the SPV and MHP except for the synchronization, power angle reset condition, and load change condition as can be seen in figure 11. The grid interconnection of the hybrid system can be studied as further work. Moreover, improved SV can be integrated into the system to obtain better frequency regulation. The voltage stability of the hybrid system can be studied for the balanced voltage profile for different scenarios. Figure 10: Load-sharing and load voltage profile on the addition of induction motor as load. During addition of motor load, voltage sags slightly as can be seen in right side.

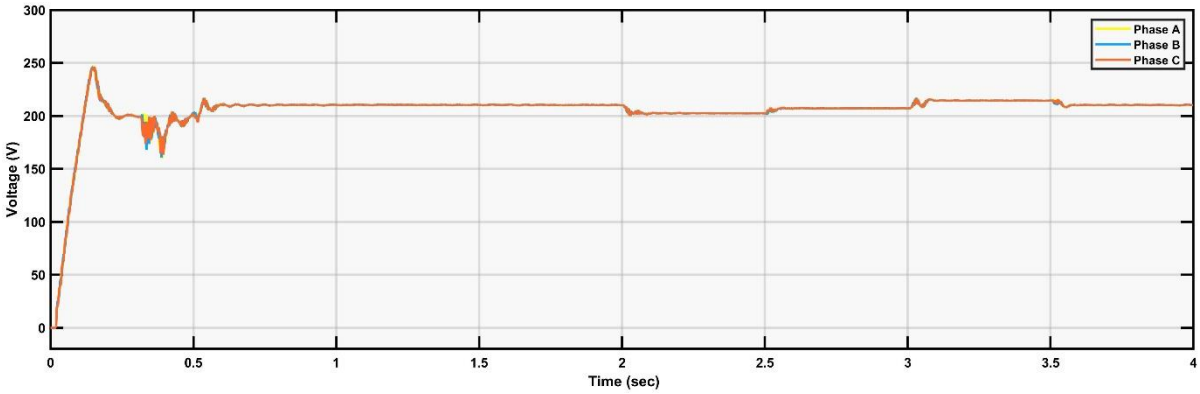

Figure 30: System load RMS voltage on the implementation of induction motor as load.

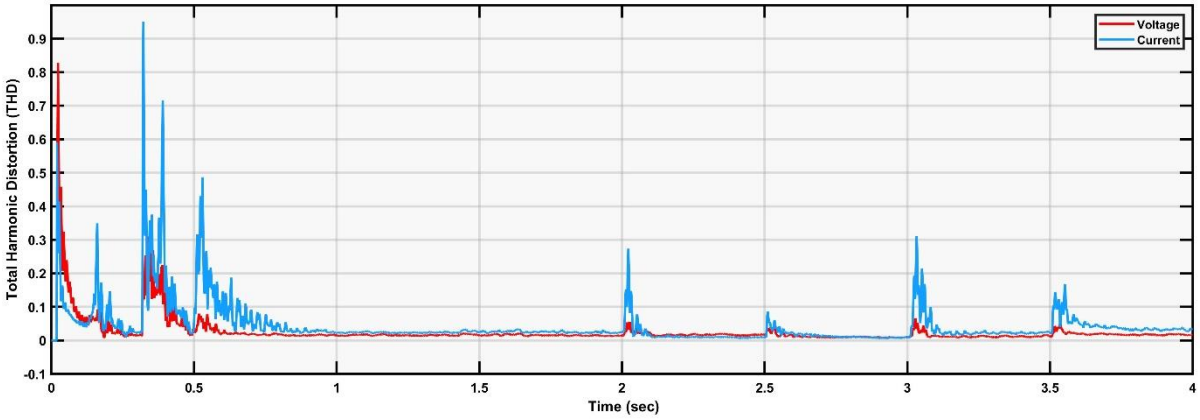

Figure 31: Total harmonic distortion of the grid voltage due to the implementation of induction motor.

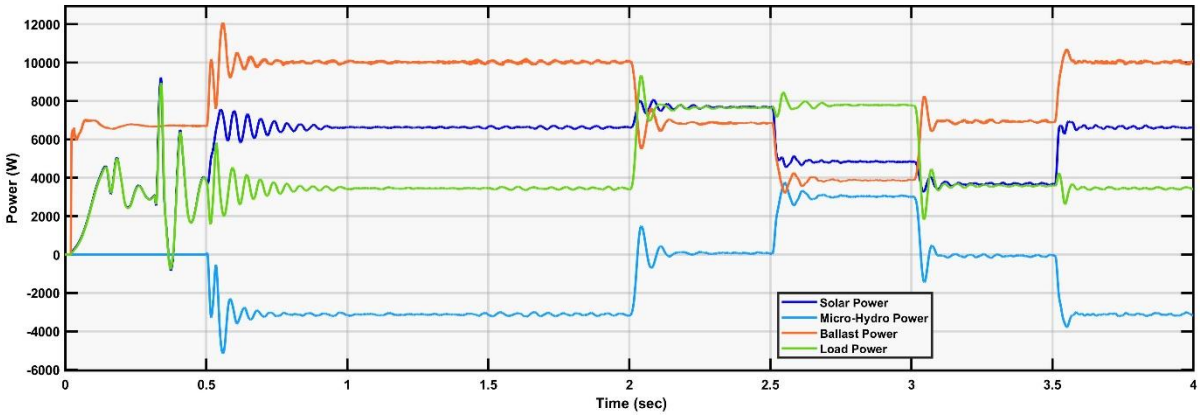

Figure 32: Load sharing by Solar PV and MHP with induction motor as load.

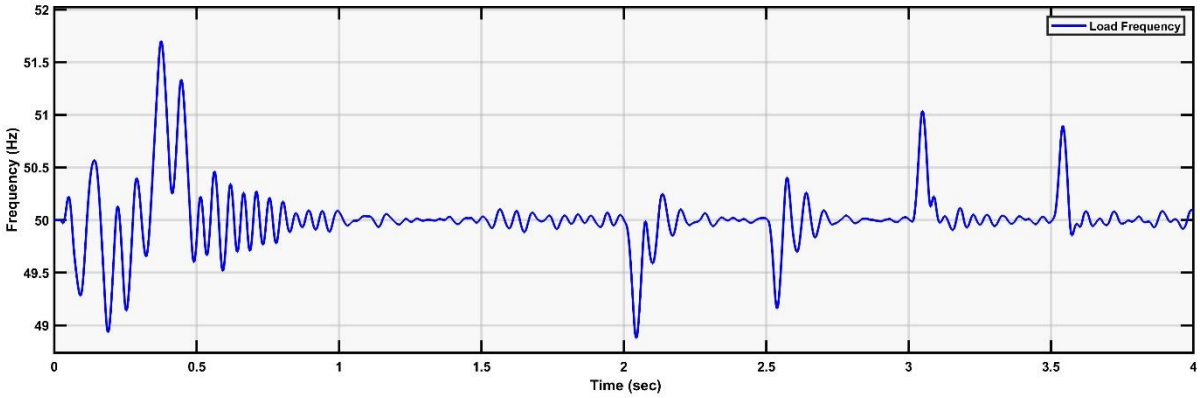

Figure 33: Frequency variation of the hybrid system on implementation of induction motor loading.

The frequency of the system oscillates for small period of time before motor comes to steady state. Voltage harmonics is seen to be high relative to current harmonics when induction motor is in operation.

CHAPTER FIVE: DISCUSSION AND FUTURE WORKS

In this study, a methodology for designing an optimal stand-alone hybrid solar-micro hydropower generating system has been proposed for 25 years of operation. This system is designed for the data of a typical remote area of Nepal that possesses the possibility of the availability of good solar irradiance with adequate streamflow nearby. This case has a typical situation for many similar regions around the world. In this study, batteries are also employed as energy storage systems. An optimal combination of components is achieved by different optimization algorithms. The optimization problem is subject to technical constraints, and finally, the configuration of components as storage-based or without storage-based with considered constraints has been compared. The financial aspect of the system is analyzed based on financial indices such as the payback period and cost of energy. Three different popular optimization algorithms have been compared based on their nature of convergence and optimal deviation. Moreover, the cost deviations for different outage rates have been analyzed. Similarly, the uncertainty effect of solar resources on the sizing of the elements has also been studied. In the future work of this study, uncertainty factors for river flow can be taken into account in calculating system cost deviation and reliability factors. Moreover, other renewable energy resources such as wind, hydrogen storage, and so on can also be used in the analysis.

Additionally, the dynamic model of the SV-based MHP hybrid system has been realized using the load sharing strategy of the power angle control method. In both load variation and irradiance variation scenarios, the system has a balanced frequency. The response load-sharing mechanism in both of the sources is observed. The application of induction motor load with a step-change in load torque concludes that the system can handle both linear and nonlinear loads with minimal frequency deviations for a short time. The synchronization can be easily obtained by resetting the virtual angle to the MHP voltage angle with added load angle for its step (sampling) time. The change in irradiance level doesn't show any frequency imbalance in the system through any complex frequency regulation mechanism that has not been used. Apart from transient time, the THD level of the load current and voltage for different scenarios remains within the short interval's standard limit. The grid interconnection of the hybrid system can be studied as further work. Moreover, improved SV can be integrated into the system to obtain better frequency regulation. The voltage stability of the hybrid system can be studied for the balanced voltage profile for different scenarios. Moreover, the study does not consider the voltage reference input for excitation. However, the use of inductive load on the system, which is generally happening in practical cases, causes the drop of system voltage significantly,

hence the system's performance. Therefore, the appropriate voltage regulation can also be studied. Moreover, the study has not considered the temperature effect on the optimal sizing as well as in performance analysis. The appropriated detail study with counting the temperature effect on the generation and performance of solar PV can be studied in future. Additionally, the financial sizing of the hybrid system has not considered the salvage value of the system components. Hence, the result is slightly underestimated. However, the contribution of the salvage value is relatively low and can still be considered for future studies.

References

1. Adaramola, M. S., Agelin-Chaab, M., & Paul, S. S. (2014). Analysis of hybrid energy systems for application in southern Ghana. *Energy Conversion and Management*, *88*, 284–295.

2. Akshay, R. S. R., & Abraham, R. J. (2019). Load-frequency regulation with solar PV and battery energy storage system. *International Journal of Power and Energy Systems*, *39*(1).

3. Allani, M. Y., Jomaa, M., Mezghani, D., & Mami, A. (2018). Modelling and simulation of the hybrid system PV-wind with MATLAB/SIMULINK. *2018 9th International Renewable Energy Congress (IREC)*, 1–6.

4. Amin, M., & Molinas, M. (2016). Self-synchronisation of wind farm in MMC-based HVDC system. *2016 IEEE Electrical Power and Energy Conference (EPEC)*, 1–6.

5. Anaza, S. O., Abdulazeez, M. S., Yisah, Y. A., Yusuf, Y. O., Salawu, B. U., & Momoh, S. U. (2017). Micro hydro-electric energy generation-An overview. *American Journal of Engineering Research (AJER)*, *6*(2), 5–12.

6. Ardakani, F. J., Riahy, G., & Abedi, M. (2010). Optimal sizing of a grid-connected hybrid system for north-west of Iran-case study. *2010 9th International Conference on Environment and Electrical Engineering*, 29–32.

7. Arthur, Y. D., Gyamfi, K. B., & Appiah, S. K. (2013). Probability distributional analysis of hourly solar irradiation in Kumasi-Ghana. *International Journal of Business and Social Research (IJBSR)*, *3*(3).

8. Atieh, A., Charfi, S., & Chaabene, M. (2018). Chapter 8 - Hybrid PV/Batteries Bank/Diesel Generator Solar-Renewable Energy System Design, Energy Management, and Economics. In I. Yahyaoui (Ed.), Advances in Renewable Energies and Power Technologies (pp. 257–294). Elsevier. doi: https://doi.org/10.1016/B978-0-12-812959-3.00008-3

9. Ayodele, T. R., & others. (2015). Determination of probability distribution function for modelling global solar radiation: case study of Ibadan, Nigeria. *International Journal*

of Applied Science and Engineering, *13*(3), 233–245.

10. Bank, N. R. (2019). *Macroeconomic indicators of nepal* (Issue November). Retrieved from https://www.nrb.org.np/contents/uploads/2019/12/Macroeconomic_Indicators_of_Nepal-2019-11_November_2019-new.pdf

11. Beshr, E. (2013). Comparative study of adding PV/wind energy systems to autonomus micro grid. *2013 3rd International Conference on Electric Power and Energy Conversion Systems*, 1–6.

12. Bignucolo, F., Stecca, R., & Coppo, M. (2018). Advantages of the Virtual Synchronous Machine regulation for integrating Low-Inertia Variable Renewable Generation in Transmission Systems. *2018 53rd International Universities Power Engineering Conference (UPEC)*, 1–6.

13. Bocklisch, T. (2015). Hybrid energy storage systems for renewable energy applications. *Energy Procedia*, *73*, 103–111. doi: 10.1016/j.egypro.2015.07.582

14. Boonbumroong, U., Pratinthong, N., Thepa, S., Jivacate, C., & Pridasawas, W. (2011). Particle swarm optimization for AC-coupling stand alone hybrid power systems. *Solar Energy*, *85*(3), 560–569.

15. Boyouk, N., Munzke, N., & Hiller, M. (2018). Peak shaving of a grid connected-photovoltaic battery system at helmholtz institute ulm (hiu). *2018 IEEE PES Innovative Smart Grid Technologies Conference Europe (ISGT-Europe)*, 1–5.

16. Celik, A. N. (2002). Optimisation and techno-economic analysis of autonomous photovoltaic--wind hybrid energy systems in comparison to single photovoltaic and wind systems. *Energy Conversion and Management*, *43*(18), 2453–2468.

17. Chaudhari, P., Rane, P., Bawankar, A., Shete, P., Kalange, K., Moghe, A., Panda, J., Kadrolkar, A., Gaikwad, K., Bhor, N., & others. (2015). Design of control systems for grid interconnection and power control of a grid tie inverter for microgrid application. *2015 IEEE International Conference on Signal Processing, Informatics, Communication and Energy Systems (SPICES)*, 1–5.

18. Cheema, K. M. (2020). A comprehensive review of virtual synchronous generator. *International Journal of Electrical Power \& Energy Systems*, *120*, 106006.

19. D'Arco, S., Suul, J. A., & Fosso, O. B. (2015). A Virtual Synchronous Machine implementation for distributed control of power converters in SmartGrids. *Electric Power Systems Research*, *122*, 180–197.

20. Das, H. S., Yatim, A. H. M., Tan, C. W., & Lau, K. Y. (2016). Proposition of a PV/tidal powered micro-hydro and diesel hybrid system: A southern Bangladesh focus. *Renewable and Sustainable Energy Reviews*, *53*, 1137–1148.

21. Dawoud, Samir M, Lin, X., & Okba, M. I. (2018). Hybrid renewable microgrid optimization techniques: A review. *Renewable and Sustainable Energy Reviews*, *82*, 2039–2052.

22. Dawoud, Samir Mohammed, Lin, X. N., Sun, J. W., Okba, M. I., Khalid, M. S., & Waqar, A. (2015). Feasibility study of isolated PV-wind hybrid system in Egypt. *Advanced Materials Research*, *1092*, 145–151.

23. Elsavad, M. A., Sarhan, A. G. M., & Abdin, A. A. M. (2017). Power angle control of virtual synchronous generator. *Journal of Electrical Engineering*, *17*(2), 2.

24. Freitas, W., Vieira, J. C. M., Morelato, A., Da Silva, L. C. P., Da Costa, V. F., & Lemos, F. A. B. (2006). Comparative analysis between synchronous and induction machines for distributed generation applications. *IEEE Transactions on Power Systems*, *21*(1), 301–311.

25. Fu, R., Feldman, D. J., & Margolis, R. M. (2018). *US solar photovoltaic system cost benchmark: Q1 2018*.

26. Fusheng, L., Ruisheng, L., & Fengquan, Z. (2016). Overview of microgrid. *Microgrid Technology and Engineering Application*, 1–10. doi: 10.1016/b978-0-12-803598-6.00001-2

27. Garche, J., Dyer, C. K., Moseley, P. T., Ogumi, Z., Rand, D. A. J., & Scrosati, B. (2013). *Encyclopedia of electrochemical power sources*. Newnes.

28. Group, I. W., & others. (1992). Recommended practice for excitation system models for power system stability studies. *IEEE Std 421.5-1992*.

29. Guwaeder, A., & Ramakumar, R. (2017). Statistical analysis of pv insolation data. *2017 IEEE 44th Photovoltaic Specialist Conference (PVSC)*, 1122–1126.

30. Harvey, A., Brown, A., Hettiarachi, P., & Inversin, A. (1993). *Micro-hydro design manual*.

31. Hatziargyriou, N., Jenkins, N., Strbac, G., Lopes, J. A. P., Ruela, J., Engler, A., Oyarzabal, J., Kariniotakis, G., Amorim, A., & others. (2006). Microgrids--large scale integration of microgeneration to low voltage grids. *CIGRE C6-309*, 1–8.

32. IEEE Guide for Synchronous Generator Modeling Practices and Parameter Verification with Applications in Power System Stability Analyses. (2020). In IEEE Std 1110-2019 (Revision of IEEE Std 1110-2002) (pp. 1–92). doi: 10.1109/IEEESTD.2020.9020274

33. Jayachandran, M., & Ravi, G. (2017). Design and Optimization of Hybrid Micro-Grid System. *Energy Procedia*, *117*, 95–103. doi: https://doi.org/10.1016/j.egypro.2017.05.111

34. Kathiresan, A. C., PandiaRajan, J., Sivaprakash, A., Sudhakar Babu, T., Islam, M., & others. (2020). An Adaptive Feed-Forward Phase Locked Loop for Grid Synchronization of Renewable Energy Systems under Wide Frequency Deviations. *Sustainability*, *12*(17), 7048.

35. Kenfack, J., Neirac, F. P., Tatietse, T. T., Mayer, D., Fogue, M., & Lejeune, A. (2009). Microhydro-PV-hybrid system: Sizing a small hydro-PV-hybrid system for rural electrification in developing countries. *Renewable Energy*, *34*(10), 2259–2263.

36. Khatod, D. K., Pant, V., & Sharma, J. (2009). Analytical approach for well-being assessment of small autonomous power systems with solar and wind energy sources. *IEEE Transactions on Energy Conversion*, *25*(2), 535–545.

37. Koutroulis, E., Kolokotsa, D., Potirakis, A., & Kalaitzakis, K. (2006). Methodology for optimal sizing of stand-alone photovoltaic/wind-generator systems using genetic algorithms. *Solar Energy*, *80*(9), 1072–1088.

38. KRISTOFERSON, L. A., & BOKALDERS, V. (1986). 22 - SMALL-SCALE HYDROPOWER. In L. A. KRISTOFERSON & V. BOKALDERS (Eds.), Renewable Energy Technologies (pp. 251–268). Pergamon. doi: https://doi.org/10.1016/B978-0-08-034061-6.50028-7

39. Kumar, S., Kaur, T., Arora, M. K., & Upadhyay, S. (2019). Resource estimation and sizing optimization of PV/micro hydro-based hybrid energy system in rural area of Western Himalayan Himachal Pradesh in India. *Energy Sources, Part a: Recovery, Utilization, and Environmental Effects*, *41*(22), 2795–2807.

40. Kumar, Y. V. P., & Bhimasingu, R. (2014). Optimal sizing of microgrid for an urban community building in south India using HOMER. *2014 IEEE International Conference on Power Electronics, Drives and Energy Systems (PEDES)*, 1–6.

41. Kusakana, K., Munda, J. L., & Jimoh, A. A. (2009). Feasibility study of a hybrid PV-micro hydro system for rural electrification. *AFRICON 2009*, 1–5.

42. Kusakana, K., & Vermaak, H. J. (2011). Hybrid Photovoltaic-Wind system as power solution for network operators in the DR Congo. *2011 International Conference on Clean Electrical Power (ICCEP)*, 703–708.

43. Lasseter, R., Akhil, A., Marnay, C., Stephens, J., Dagle, J., Guttromson, R., Meliopoulous, A., Yinger, R., & Eto, J. (2002). The CERTS microgrid concept. *White Paper for Transmission Reliability Program, Office of Power Technologies, US Department of Energy*, *2*(3), 30.

44. Lasseter, R. H., & Paigi, P. (2004). Microgrid: A conceptual solution. *2004 IEEE 35th Annual Power Electronics Specialists Conference (IEEE Cat. No. 04CH37551)*, *6*, 4285–4290.

45. Lazzeroni, P., & Repetto, M. (2019). Optimal planning of battery systems for power losses reduction in distribution grids. *Electric Power Systems Research*, *167*, 94–112.

46. Liu, J., Yang, D., Yao, W., Fang, R., Zhao, H., & Wang, B. (2017). PV-based virtual synchronous generator with variable inertia to enhance power system transient stability utilizing the energy storage system. *Protection and Control of Modern Power Systems*, *2*(1), 1–8.

47. Lv, Y., Guan, L., Tang, Z., & Zhao, Q. (2016). A probability model of PV for the middle-term to long-term power system analysis and its application. *Energy Procedia*, *103*, 28–33.

48. Maharjan, S., & Shrestha, R. (2014). Technical problem analysis of micro hydro plants: A case study at Pokhari Chauri of Kavre District. *Journal of the Institute of Engineering*, *10*(1), 149–156.

49. Majumder, R., Ghosh, A., Ledwich, G., & Zare, F. (2009). Angle droop versus frequency droop in a voltage source converter based autonomous microgrid. *2009 IEEE Power and Energy Society General Meeting, PES '09*. doi: 10.1109/PES.2009.5275987

50. Marnay, C., Chatzivasileiadis, S., Abbey, C., Iravani, R., Joos, G., Lombardi, P., Mancarella, P., & von Appen, J. (2015). Microgrid evolution roadmap. *2015 International Symposium on Smart Electric Distribution Systems and Technologies (EDST)*, 139–144.

51. Menon, M. K. D. (2016). A novel method to extract maximum power from solar panel of a grid connected phototvoltaic system using phase angle control and hysteresis current control. *2016 International Conference on Electrical, Electronics, and Optimization Techniques (ICEEOT)*, 3510–3516.

52. Meshram, S., Agnihotri, G., & Gupta, S. (2014). Advanced photovoltaic/hydro hybrid renewable energy system for remote areas. *Journal of Renewable and Sustainable Energy*, *6*(1), 13140.

53. Meyer, T. (2004). *Photovoltaic energy: Stand-alone and grid-connected systems*.

54. MoghaddasTafreshi, S. M., & Hakimi, S. M. (2007). Optimal sizing of a stand-alone hybrid power system via particle swarm optimization (PSO). *2007 International Power Engineering Conference (IPEC 2007)*, 960–965.

55. Mohammadi, M., Hosseinian, S. H., & Gharehpetian, G. B. (2012). GA-based optimal sizing of microgrid and DG units under pool and hybrid electricity markets. *International Journal of Electrical Power \& Energy Systems*, *35*(1), 83–92.

56. Mover, W. G. P., & Supply, E. (1992). Hydraulic turbine and turbine control models

for system dynamic studies. *IEEE Transactions on Power Systems*, *7*(1), 167–179.

57. Murni, S., Whale, J., Urmee, T., Davis, J., & Harries, D. (2012). The role of micro hydro power systems in remote rural electrification: a case study in the Bawan Valley, Borneo. *Procedia Engineering*, *49*, 189–196.

58. NEA. (2018). *Nepal Electricity Authority Report*. Retrieved from https://www.nea.org.np/admin/assets/uploads/supportive_docs/annual_report_2076.pdf

59. of Electrical, I., & Committee, E. E. S. P. C. (1981). *IEEE Guide for Harmonic Control and Reactive Compensation of Static Power Converters*. Ieee.

60. Pearsall, N. M. (2017). 1 - Introduction to photovoltaic system performance. In N. Pearsall (Ed.), The Performance of Photovoltaic (PV) Systems (pp. 1–19). Woodhead Publishing. doi: https://doi.org/10.1016/B978-1-78242-336-2.00001-X

61. Rahimpour, M. R., Kazerooni, N. M., & Parhoudeh, M. (2019). Chapter 8 - Water Treatment by Renewable Energy-Driven Membrane Distillation. In A. Basile, A. Cassano, & A. Figoli (Eds.), Current Trends and Future Developments on (Bio-) Membranes (pp. 179–211). Elsevier.

62. Rai, S. K., Rahi, O. P., & Kumar, S. (2015). Implementation of electronic load controller for control of micro hydro power plant. *2015 International Conference on Energy Economics and Environment (ICEEE)*, 1–6.

63. Ramoji, S. K., Rath, B. B., & Kumar, D. V. (2014). Optimization of hybrid PV/wind energy system using genetic algorithm (GA). *Journal of Engineering Research and Applications*, *4*, 29–37.

64. Razmjoo, A., Shirmohammadi, R., Davarpanah, A., Pourfayaz, F., & Aslani, A. (2019). Stand-alone hybrid energy systems for remote area power generation. *Energy Reports*, *5*, 231–241.

65. *Renewable Power Generation Costs in 2019*. (2020). IRENA. Retrieved from https://www.irena.org/publications/2020/Jun/Renewable-Power-Costs-in-2019

66. Ruan, X., Wang, X., Pan, D., Yang, D., Li, W., & Bao, C. (2018). Design of LCL filter. In Control Techniques for LCL-Type Grid-Connected Inverters (pp. 31–61). Springer.

67. Salmi, T., Bouzguenda, M., Gastli, A., & Masmoudi, A. (2012). Matlab/simulink based modeling of photovoltaic cell. *International Journal of Renewable Energy Research (IJRER)*, *2*(2), 213–218.

68. Shah, H., Ghazali, R., Herawan, T., Rahman, S. U., & Khan, N. (2016). Chapter 14 - Swarm Based-Artificial Neural System for Human Health Data Classification. In D. Al-Jumeily, A. Hussain, C. Mallucci, & C. Oliver (Eds.), Applied Computing in Medicine and Health (pp. 287–309). Boston: Morgan Kaufmann. doi: https://doi.org/10.1016/B978-0-12-803468-2.00014-X

69. Singh, B., Kasal, G. K., & Gairola, S. (2008). Power quality improvement in conventional electronic load controller for an isolated power generation. *IEEE Transactions on Energy Conversion*, *23*(3), 764–773.

70. Singh, S., Verma, R. K., Shakya, A. K., & Singh, S. P. (2016). Frequency stability analysis of hybrid power system based on solar PV with SMEs unit. *2016 International Conference on Emerging Trends in Electrical Electronics \& Sustainable Energy Systems (ICETEESES)*, 5–11.

71. Sinha, S., & Chandel, S. S. (2017). Improving the reliability of photovoltaic-based hybrid power system with battery storage in low wind locations. *Sustainable Energy Technologies and Assessments*, *19*, 146–159.

72. Soni, V. K., & Khare, R. (2014). Optimal sizing of HRES for small sized institute using HOMER. *2014 IEEE 2nd International Conference on Electrical Energy Systems (ICEES)*, 77–81.

73. *Streamflow Prediction Tool, Nepal*. (n.d.). ICIMOD. Retrieved from https://servir.icimod.org/science-applications/streamflow-prediction-tool-nepal

74. Svensson, J. (1995). *Power angle control of grid-connected voltage source converter in a wind energy application.*

75. Syahputra, R., & Soesanti, I. (2021). Renewable energy systems based on micro-hydro

and solar photovoltaic for rural areas: A case study in Yogyakarta, Indonesia. *Energy Reports*, *7*, 472–490.

76. Thieu, N. Van. (2020). *A collection of the state-of-the-art MEta-heuristics ALgorithms in PYthon: Mealpy*. Zenodo. doi: 10.5281/zenodo.3711948

77. Ton, D. T., & Smith, M. A. (2012). The US department of energy's microgrid initiative. *The Electricity Journal*, *25*(8), 84–94.

78. Tsai, H.-L., Tu, C.-S., Su, Y.-J., & others. (2008). Development of generalized photovoltaic model using MATLAB/SIMULINK. *Proceedings of the World Congress on Engineering and Computer Science*, *2008*, 1–6.

79. Vaidya, D. (2014). Cost and revenue structures for micro-hydro projects in nepal. *Paper Prepared by Dr. Vaidya, Micro-Hydro Specialist under Contract with AEPC Cost Structure of Micro Hydropower Plant*.

80. van Rossum, G. (1995). *Python tutorial* (Issue CS-R9526). Amsterdam.

81. Vijayakumari, A., Devarajan, A. T., & Mohanrajan, S. R. (2016). Power angle control of a single phase grid connected photovoltaic inverter for controlled power transfer. *Proceedings of the International Conference on Soft Computing Systems*, 451–461.

82. Vuc, G., Borlea, I., Barbulescu, C., Prostean, O., Jigoria-Oprea, D., & Neaga, L. (2011). Optimal energy mix for a grid connected hybrid wind Photovoltaic generation system. *EXPRES 2011 - 3rd IEEE International Symposium on Exploitation of Renewable Energy Sources, Proceedings*, *January 2019*, 129–132. doi: 10.1109/EXPRES.2011.5741806

83. Xu, D., Kang, L., Chang, L., & Cao, B. (2005). Optimal sizing of standalone hybrid wind/PV power systems using genetic algorithms. *Canadian Conference on Electrical and Computer Engineering*, *2005.*, 1722–1725.

84. Xue, Y., Deng, J., & Ma, S. (2009). Power flow control of a distributed generation unit in micro-grid. *2009 IEEE 6th International Power Electronics and Motion Control Conference*, 2122–2125.

85. Yang, H., Wei, Z., & Chengzhi, L. (2009). Optimal design and techno-economic analysis of a hybrid solar--wind power generation system. *Applied Energy*, *86*(2), 163–169.

86. Yang, H., Zhou, W., Lu, L., & Fang, Z. (2008). Optimal sizing method for stand-alone hybrid solar--wind system with LPSP technology by using genetic algorithm. *Solar Energy*, *82*(4), 354–367.

87. Yap, K. Y., Sarimuthu, C. R., & Lim, J. M.-Y. (2019). Virtual inertia-based inverters for mitigating frequency instability in grid-connected renewable energy system: A review. *Applied Sciences*, *9*(24), 5300.

88. Yimen, N., Tchotang, T., Kanmogne, A., Abdelkhalikh Idriss, I., Musa, B., Aliyu, A., Okonkwo, E. C., Abba, S. I., Tata, D., Meva'a, L., & others. (2020). Optimal Sizing and Techno-Economic Analysis of Hybrid Renewable Energy Systems—A Case Study of a Photovoltaic/Wind/Battery/Diesel System in Fanisau, Northern Nigeria. *Processes*, *8*(11), 1381.

89. Zhong, Q.-C., & Hornik, T. (2012). *Control of power inverters in renewable energy and smart grid integration* (Vol. 97). John Wiley \& Sons.

90. Zhong, Q.-C., & Weiss, G. (2010). Synchronverters: Inverters that mimic synchronous generators. *IEEE Transactions on Industrial Electronics*, *58*(4), 1259–1267.

91. Zolfaghari, M., Ghaffarzadeh, N., & Ardakani, A. J. (2019). Optimal sizing of battery energy storage systems in off-grid micro grids using convex optimization. *Journal of Energy Storage*, *23*, 44–56.

APPENDIX A: Python Program for Generation Modelling for Optimal Sizing

```
import numpy as np
import pandas as pd
import matplotlib.pyplot as plt

data = pd.read_csv('https://raw.githubusercontent.com/deependran7/Datasets/master/hourly_data.csv')
I_r = data.ghi.to_list()
Q = data.discharge.to_list()
P_load = data.p.to_list()
Q_load = data.q.to_list()
K_load = data.kva.to_list()
w_speed = data.wind_speed.to_list()
data = data.set_index('date')

class Hydro_model:
    mhp_cc = 1777
    mhp_om = 53.31
    Q_des = 0
    dr = 0.1;
    n = 25;
    crf = (dr*(1+dr)**n)/(((1+dr)**n)-1);

    def __init__(self, eta_mhp,gamma,q,h):
        self.eta_mhp = eta_mhp
        self.gamma = gamma
        self.q = q
        self.h = h
    def set_Q_des(self, Q_des):
        self.Q_des = Q_des
    def set_H_des(self,h):
        self.h = h
    def Power(self):
        power = [0]*len(self.q)
```

```
        for k in range(len(self.q)):
            if self.q[k] <= self.Q_des:
                power[k] = self.eta_mhp*self.gamma*self.q[k]*self.h
            else:
                power[k] = self.eta_mhp*self.gamma*self.Q_des*self.h
        return np.array(power)
    def Cost(self):
        Power = self.eta_mhp*self.gamma*self.Q_des*self.h
        return Power*(self.mhp_cc + self.mhp_om/self.crf);

class PV_model:
    pv_cc = 618;
    pv_om = 10;
    dr = 0.1;
    n = 25;
    crf = (dr*(1+dr)**n)/(((1+dr)**n)-1);

    def __init__(self, N_pv,I_r):
        self.N_pv = N_pv
        self.I_r = I_r
    def Power(self):
        power = [0]*len(self.I_r)
        for k in range(len(self.I_r)):
            power[k] = self.N_pv*(self.I_r[k]/1000)
        return np.array(power)
    def Cost(self):
        return self.N_pv * (self.pv_cc +self.pv_om/self.crf);

labels = ['Jan','Feb','Mar','Apr','May','Jun','Jul','Aug','Sep', 'Oct','Nov','Dec']
x = np.arange(730/2,730*12, 730)

fig,ax1 = plt.subplots(1,1)
fig.set_size_inches(10,4)
plt.plot(I_r)
plt.xlim([0, 7*24])
```

```
plt.ylim(-5,1500)
plt.xlabel('Month')
plt.ylabel('Global Horizontal Irridance')
plt.grid(False)
ax1.legend(['$kWh/m^2$'],loc='upper right',frameon=False, ncol=3)
ax1.set_xticks(x)
ax1.set_xticklabels(labels)
plt.savefig('solar.jpeg',bbox_inches = 'tight',dpi = 300)
plt.show()


labels = ['Jan','Feb','Mar','Apr','May','Jun','Jul','Aug','Sep', 'Oct','Nov','Dec']
x = np.arange(730/2,730*12, 730)

fig,ax1 = plt.subplots(1,1)
fig.set_size_inches(10,4)
plt.plot(Q)
plt.xlim([0, 7*24])
plt.ylim(-1,30)
plt.xlabel('Month')
plt.ylabel('Stream Discharge ')
plt.grid(False)
ax1.legend(['$m^3/sec$'],loc='upper right',frameon=False, ncol=3)
ax1.set_xticks(x)
ax1.set_xticklabels(labels)
plt.savefig('discharge.jpeg',bbox_inches = 'tight',dpi = 300)
plt.show()
labels = ['Jan','Feb','Mar','Apr','May','Jun','Jul','Aug','Sep', 'Oct','Nov','Dec']
x = np.arange(730/2,730*12, 730)

class Load_model:
    def __init__(self, load_profile,factor):
        self.loading = np.array(load_profile)*factor
    def Power(self):
        return self.loading
```

```
pload = Load_model(P_load,0.4)
qload = Load_model(Q_load,0.4)
sload = Load_model(K_load,0.4)

labels = ['Sunday','Monday','Tuesday','Wednesday','Thrusday','Friday','Saturday']
x = np.arange(12,7*24, 24)

fig,ax1 = plt.subplots(1,1)
fig.set_size_inches(10,4)
plt.plot(pload.Power())
plt.plot(qload.Power())
plt.plot(sload.Power())
plt.xlim([0, 7*24])
plt.ylim(-5,40)
plt.xlabel('Day')
plt.ylabel('Loading')
plt.grid(False)
ax1.legend(['KW', 'KVar', 'KVa'],loc='lower center',frameon=False, ncol=3)
ax1.set_xticks(x)
ax1.set_xticklabels(labels)
plt.savefig('loading.jpeg',bbox_inches = 'tight',dpi = 300)
plt.show()
#files.download('loading.png')

class Battery_model:
    sigma = 0.0001
    eta_inv = 0.9
    eta_bd = 0.9
    eta_bc = 0.9
    C_b = 2.42
    DOD = 0.8
    Soc = [0.5]*8761
    P_bat = [0]*8761
    nb_cc = 200
```

```
nb_om = 0
nb_rep = 200
dr = 0.1;
n = 25;
crf = (dr*(1+dr)**n)/(((1+dr)**n)-1);

def __init__(self, N_b,Delta_P):
    self.N_b  = N_b
    self.Delta_P = Delta_P

def SOC(self):
    for k in range(1,len(self.Delta_P)):
        if self.Delta_P[k-1] > 0:
            if self.Soc[k-1] >=1:
                self.Soc[k] = 1

            else:
                if self.Delta_P[k-1] >=self.N_b*self.C_b:
                    power = self.N_b*self.C_b
                    self.Soc[k] = self.Soc[k-1]*(1-self.sigma) + (power)*self.eta_bc/(self.N_b*self.C_b)

                else:
                    power = self.Delta_P[k-1]
                    self.Soc[k] = self.Soc[k-1]*(1-self.sigma) + (power)*self.eta_bc/(self.N_b*self.C_b)

            if self.Soc[k]>=1:
                self.Soc[k] = 1

        if self.Delta_P[k-1] < 0:
            if (self.Soc[k-1])<= (1-self.DOD):
                self.Soc[k] = 1-self.DOD

            else:
                self.Soc[k] = self.Soc[k-1]*(1-self.sigma)+ self.Delta_P[k-1]/(self.eta_bd*self.N_b*self.C_b)
                self.P_bat[k]=-self.Delta_P[k]
```

```
            if (self.Soc[k] <=(1-self.DOD)):
                self.Soc[k] = 1-self.DOD
        return np.array(self.Soc)


    def Power(self):
        self.SOC()
        for k in range(1,len(self.Delta_P)):
            if self.Soc[k-1] >= self.Soc[k]:
                #battery discharges
                self.P_bat[k-1] = (self.Soc[k-1]-self.Soc[k]*(1-self.sigma))*self.eta_bd*self.N_b*self.C_b
            else:
                #battery charges
                self.P_bat[k-1] = (self.Soc[k-1]-self.Soc[k]*(1-self.sigma))*self.eta_bc*self.N_b*self.C_b
        return np.array(self.P_bat)

    def calc_rep(self):
        return (1/(1+self.dr)**5 + 1/(1+self.dr)**10 + 1/(1+self.dr)**15 + 1/(1+self.dr)**20)

    def Cost(self):
        return self.N_b * (self.nb_cc +self.nb_om/self.crf) + self.N_b * self.nb_rep * self.calc_rep() ;

class ELC:
    elc_r = 0
    cc_elc= 150
    om_elc=150*5/100
    dr = 0.1;
    n = 25;
    crf = (dr*(1+dr)**n)/(((1+dr)**n)-1);
    def __init__(self,load,battery,*Power_sources):
        self.Power_sources = Power_sources
        self.load = load
        self.battery = battery

    def Power(self):
```

```
        residual_power = 0
        for power_source in self.Power_sources:
            residual_power = residual_power + power_source.Power()
        return residual_power-self.load.Power()+self.battery.Power()
    def Cost(self):
        self.elc_r = max(self.Power())
        return (self.elc_r*self.cc_elc + self.om_elc * self.elc_r/self.crf )

class Inverter_model:
  eta_inv = 0.98
  inv_cc = 200
  inv_om = 0
  inv_rep = 200
  dr = 0.1;
  def __init__(self, Battery_model, pf):
    self.Battery_model = Battery_model
    self.pf  = pf

  def Power(self):
    return self.Battery_model.Power()*self.eta_inv

  def calc_rep(self):
      return (1/(1+self.dr)**10 + 1/(1+self.dr)**20)

  def calc_kva(self):
    return self.Battery_model.N_b * self.Battery_model.C_b/self.pf
  def Cost(self):
    return (self.inv_cc * self.calc_kva() +self.inv_rep*self.calc_kva()*self.calc_rep())
```

APPENDIX B: Python Program for Optimization Formulation and Solution

```
"""<h3>Optimisation Algorithmis</h3>

<h5>We are using Memetic Algrithm, particle swarm optimisation, genetic algorithm and articifical bee cololy optimisation</h5> """

from mealpy.evolutionary_based.GA import BaseGA

from mealpy.swarm_based.PSO import BasePSO

from mealpy.swarm_based.ABC import BaseABC


def Loss_function(x=None):
    hydro = Hydro_model(0.5,9.8,Q,30)
    hydro.set_Q_des(x[1])
    hydro.set_H_des(x[2])
    solar = PV_model(x[0], I_r)
    load = Load_model(P_load,0.4)
    delta_P = hydro.Power() + solar.Power() - load.Power()
    battery = Battery_model(x[3],delta_P)
    elc = ELC(load,battery,hydro,solar)
    inv = Inverter_model(battery, 0.85)
    outage = 0
    el = elc.Power()
    for k in range(len(I_r)):
        out = el[k]
        if out < 0:
            outage = outage + 1
    #print(outage)
    if (outage) == 0:
        z = hydro.Cost() + solar.Cost() + battery.Cost() + inv.Cost()
        return z
    else:
        return 100000000


lb = [0,  0.0, 1, 0]

ub = [50, 2.0, 40,60]

problem_size = 100

batch_size = 10

verbose = True
```

```
epoch = 200
pop_size = 100

md = BaseMA(Loss_function, lb, ub, verbose, epoch, pop_size)
best_pos, best_fit, list_loss = md.train()
MA_sol = {
  "name": "MA",
  "best_pos": best_pos,
  "best_fit": best_fit,
  "list_loss": list_loss
}

md = BaseGA(Loss_function, lb, ub, verbose, epoch, pop_size)
best_pos, best_fit, list_loss = md.train()
GA_sol = {
  "name": "GA",
  "best_pos": best_pos,
  "best_fit": best_fit,
  "list_loss": list_loss
}

md = BasePSO(Loss_function, lb, ub, verbose, epoch, pop_size)
best_pos, best_fit, list_loss = md.train()
PSO_sol = {
  "name": "PSO",
  "best_pos": best_pos,
  "best_fit": best_fit,
  "list_loss": list_loss
}

md = BaseABC(Loss_function, lb, ub, verbose, epoch, pop_size)
best_pos, best_fit, list_loss = md.train()
ABC_sol = {
  "name": "ABC",
  "best_pos": best_pos,
```

```
  "best_fit": best_fit,
  "list_loss": list_loss
}

import matplotlib
fig,ax = plt.subplots(1,1)
fig.set_size_inches(10,4)
ax.plot(ABC_sol['list_loss'])
ax.plot(PSO_sol['list_loss'])
ax.plot(GA_sol['list_loss'])
ax.legend(['ABC','PSO','GA'])
plt.xlabel('Epochs')
plt.ylabel('Optimal Cost Solutions (USD)')
ax.get_yaxis().set_major_formatter(
    matplotlib.ticker.FuncFormatter(lambda x, p: format(int(x), ',')))
fig.tight_layout()
plt.savefig('algorithm_comparsion.png',bbox_inches = 'tight')
plt.show()

sol_data = pd.DataFrame()
sol_data['ABC'] = ABC_sol['list_loss']
sol_data['PSO'] = PSO_sol['list_loss']
sol_data['GA'] = GA_sol['list_loss']
a = ABC_sol.get('best_pos')
print(a)
a = [12.21413162,  0.12120023, 39.62723023 ,25.7872984 ]
```

APPENDIX C: MATLAB/SIMULINK Models of the Hybrid System Components.

A. Virtual Governor Model

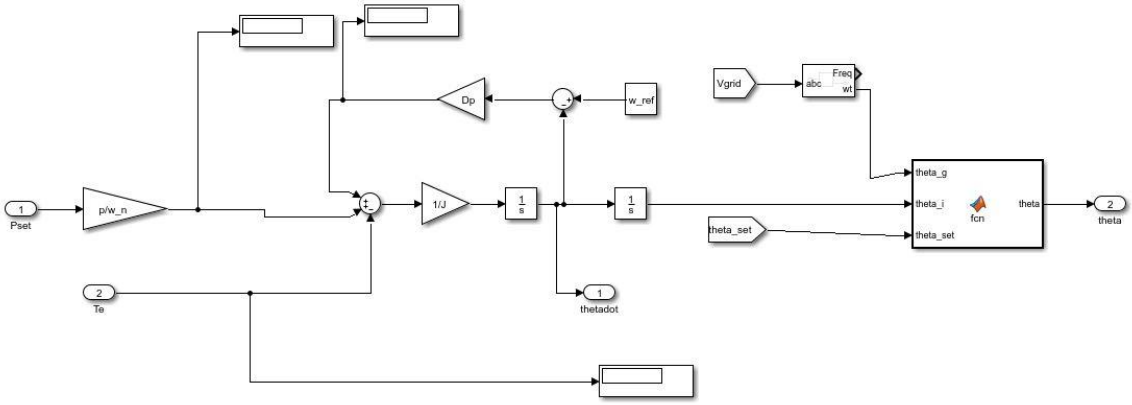

B. Virtual Excitor Model

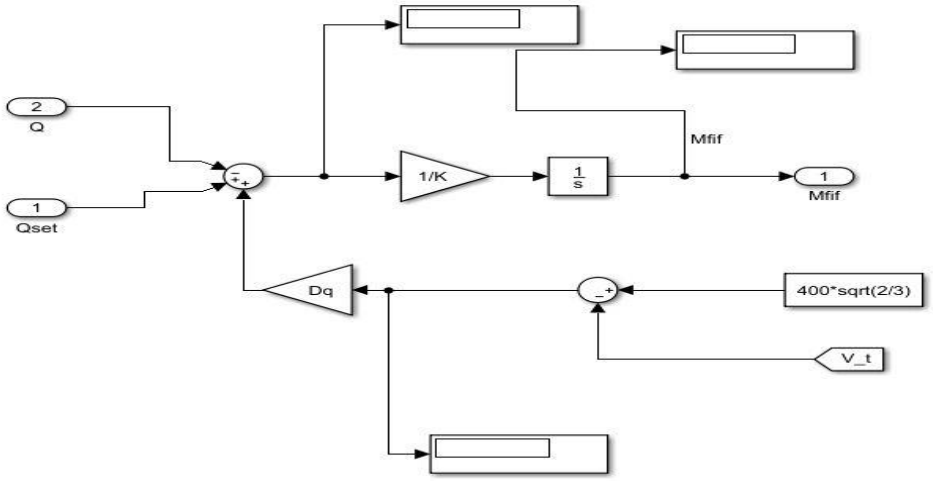

C. Solar PV Model

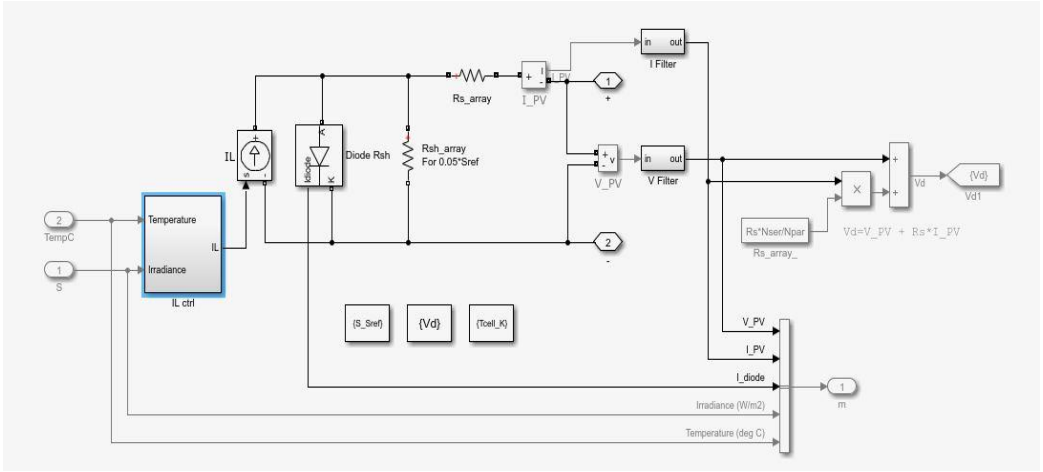

D. Solar Photo Current Model

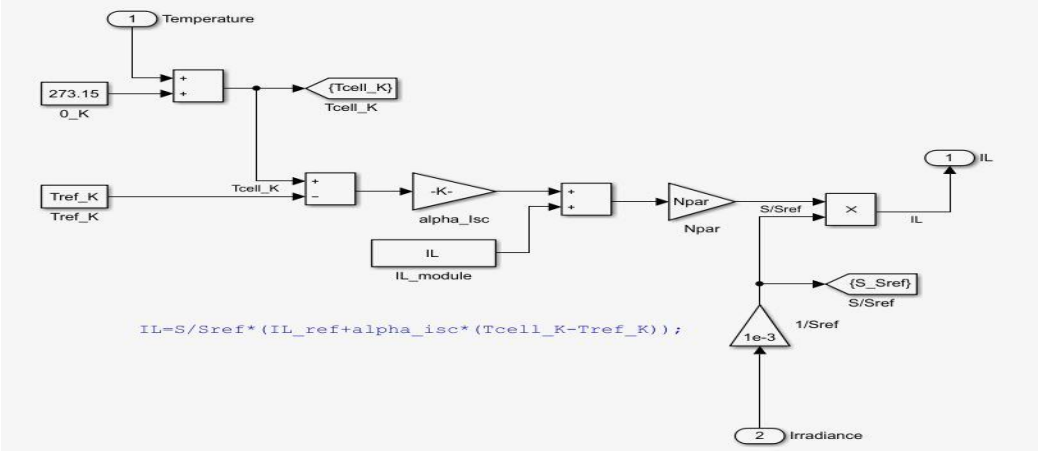

E. Pulse Generator Model

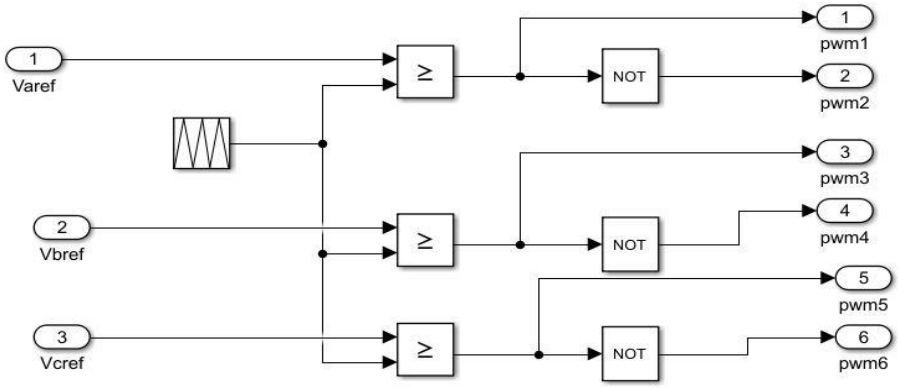

F. Overall Hybrid System Model

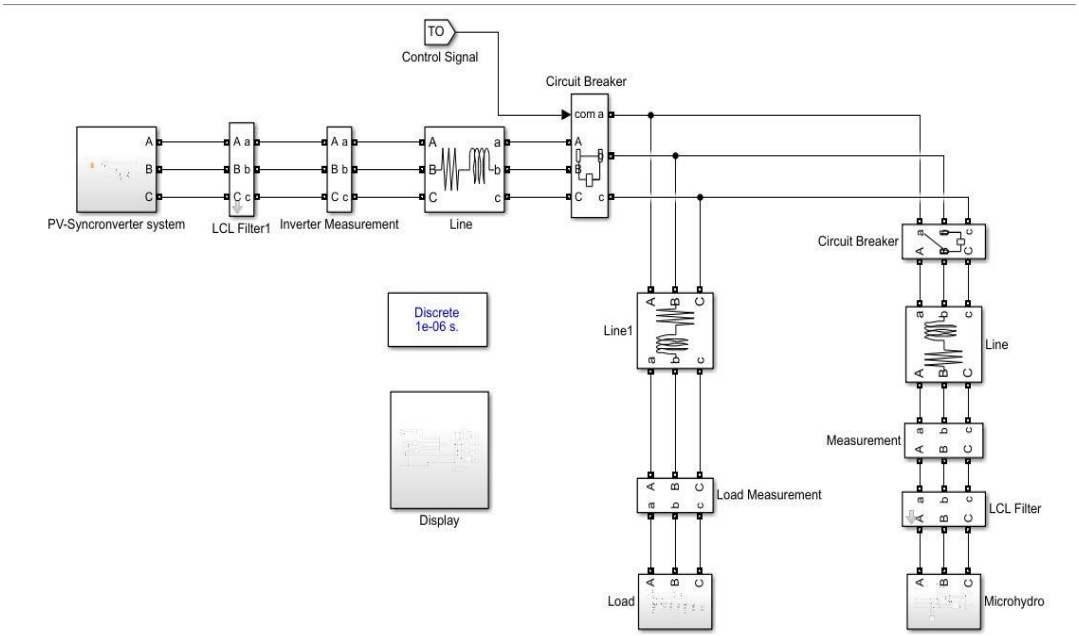

G. Micro Hydropower Model

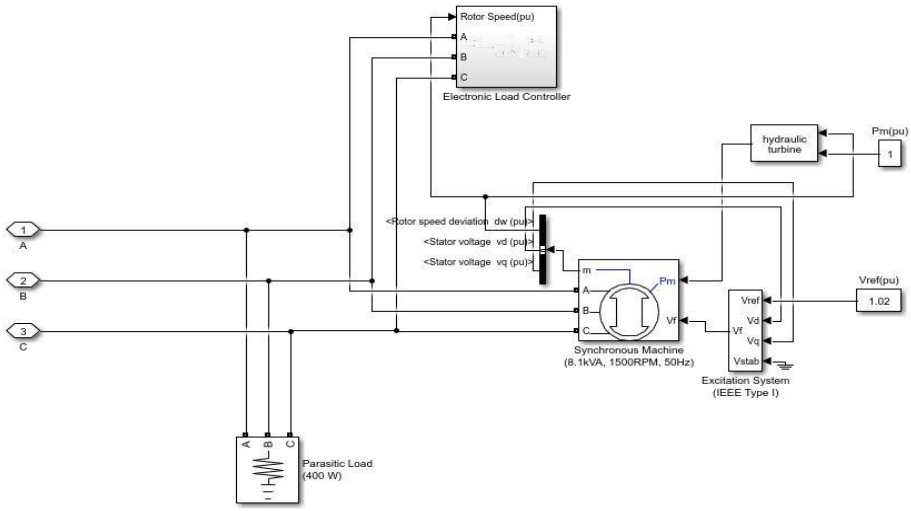

H. LCL Filter Model

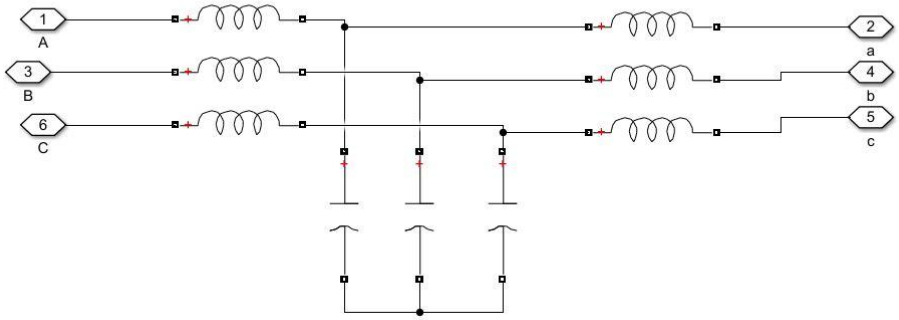

I. Power Inverter Model

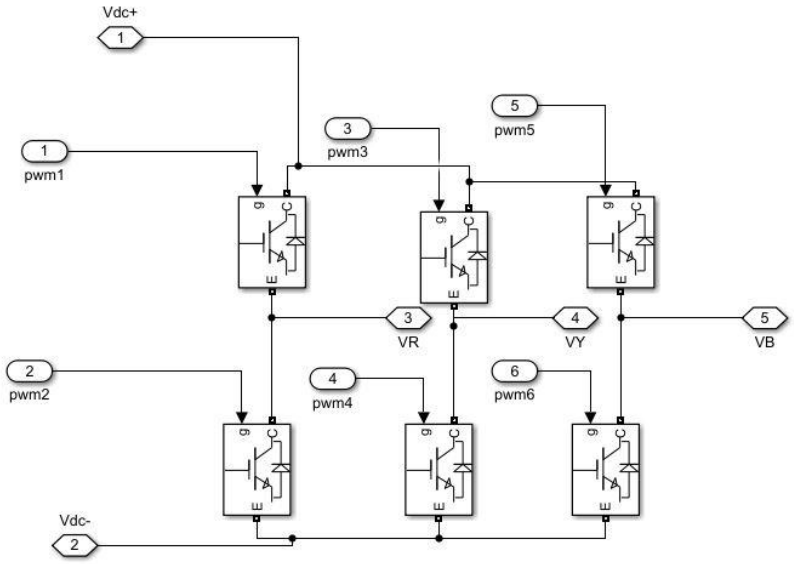

J. Electronic Load Controller Model

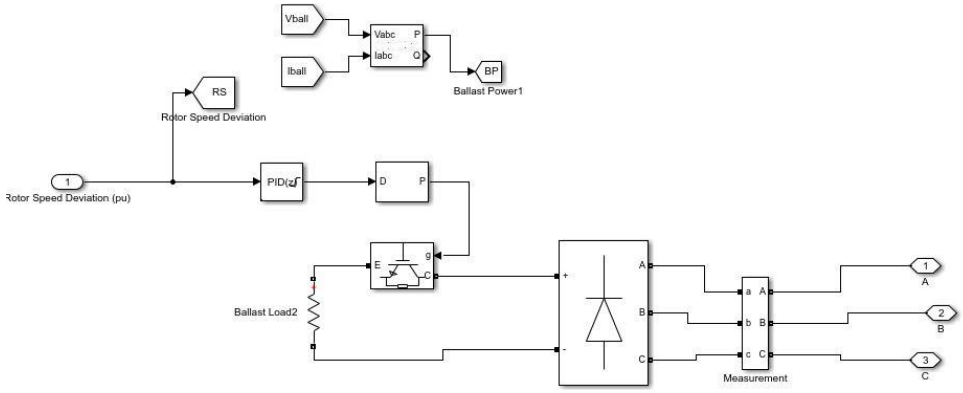

APPENDIX D: Publication

Neupane, D., Kafle, S., Gurung, S., Neupane, S., & Bhattarai, N. (2021). Optimal sizing and financial analysis of a stand-alone SPV-micro-hydropower hybrid system considering generation uncertainty. *International Journal of Low-Carbon Technologies, 16*(4), 1479-1491.

APPENDIX E: Plagiarism Test Report

Deependra_neupane

ORIGINALITY REPORT

18%
SIMILARITY INDEX

PRIMARY SOURCES

1	www.journaltocs.ac.uk Internet	140 words — 1%
2	www.ijraset.com Internet	135 words — 1%
3	www.researchsquare.com Internet	112 words — 1%
4	www.mdpi.com Internet	105 words — 1%
5	Fatemeh Jahanbani Ardakani. "Optimal sizing of a grid-connected hybrid system for north-west of Iran-case study", 2010 9th International Conference on Environment and Electrical Engineering, 05/2010 Crossref	88 words — 1%
6	Rai, Shailendra Kumar, O. P. Rahi, and Sunil Kumar. "Implementation of electronic load controller for control of micro hydro power plant", 2015 International Conference on Energy Economics and Environment (ICEEE), 2015. Crossref	67 words — < 1%
7	dokumen.pub Internet	57 words — < 1%